A Fourth Order Dual Method for Staircase Reduction in Texture Extraction and Image Restoration Problems *

Tony F. Chan† Selim Esedoglu† Frederick E. Park†

April 21, 2005

Abstract

We propose a fourth order dual method for the minimization of the non-smooth semi-norm $\|\Delta \cdot\|_1$ when in amalgamation with new staircase reducing texture decomposition and restoration models of image processing. The proposed models incorporating this high order energy include a variant of the Chambolle and Lions model for image denoising and variants of the models by Chan, Esedoglu, and Park for texture extraction and restoration problems. We claim that the dual method is faster and more stable than the current gradient descent time marching algorithms often used to minimize such energies. Moreover, proofs of convergence of the proposed method, in conjunction with the new imaging models, will be provided.

1 Introduction

Image denoising and texture extraction are two important problems in image processing that have both seen many recent developments. One of the most important building blocks for modelling such tasks is the original discontinuity (edge) preserving image denoising model proposed by Rudin, Osher, and Fatemi (ROF) [19]:

$$\min_{u\in BV(\Omega)} \int_\Omega |\nabla u| + \frac{1}{2\lambda}\int_\Omega (f-u)^2\, d\mathbf{x}. \tag{1}$$

Here f is the observed image, u the restored image, $\Omega \subset \mathbb{R}^2$ an open bounded domain (usually a rectangle in $\mathbb{R}^2$), and $BV(\Omega)$ is the space of functions of bounded variation. The ROF model has proven to be a popular image denoising model and has also seen much use in the modelling of structural (geometric) components in texture decomposition problems.

Many of the current partial differential equation (PDE) methods for image denoising and decomposition utilize TV regularization for its beneficial discontinuity (edge) preserving property. However, a particular caveat of TV regularization is the staircasing (terracing) phenomenon in recovered images. Generally speaking, staircasing occurs to the highest degree in image reconstructions by functionals that depend non-convexly on image gradients. A key example is the scheme by Perona and Malik which can be interpreted as gradient descent on a non-convex functional depending sublinearly on image gradients at infinity. The TV model is on the brinks of non-convexity; it depends linearly on image gradients at infinity. This feature has two edges, since it is responsible for its ability to reconstruct images with

*This work was partially supported by grants from the NSF under contract DMS-0410085, the ONR under contract N00014-03-1-0888, and the NIH under contract U54 RR021813.

†Department of Mathematics, University of California, 405 Hilgard Avenue, Los Angeles, CA 90095-1555. Email: {chan,esedoglu,fpark}@math.ucla.edu

discontinuities while also being responsible for staircasing. Some examples of staircasing in restorations from the ROF model can be observed in Figure 1 for the 1-d and 2-d cases; the 1-d case is included to better isolate the phenomenon.

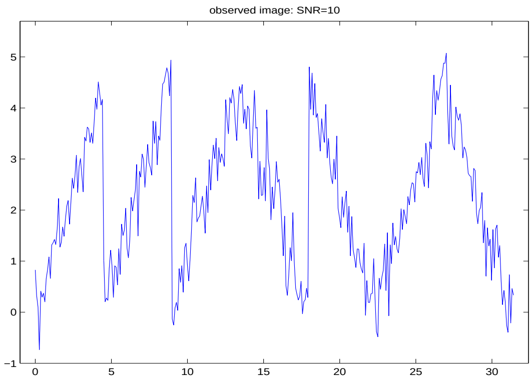

Observed Signal, SNR = 10

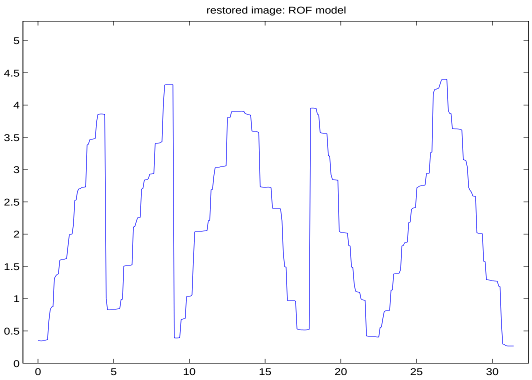

Staircasing in Recovered Signal

Observed Signal, $\sigma = 20$

Staircasing in Recovered Signal

Figure 1: *Staircasing in Recovered Signals from the ROF Model:* Top left, observed 1-d signal, SNR=10. Bottom left, observed signal, $\sigma = 20$, σ^2 denotes the variance of the Gaussian noise. Top and bottom right, recovered signals from the ROF model (1). Staircasing is observed in both recovered signals.

There are many ways to overcoming staircasing in reconstructions from TV regularization. One method is to introduce higher order derivatives into the energy as in the approach by Chambolle and Lions (CL) [9], where the authors introduce the notion of *inf convolution* between two convex functionals. Here, an image u is decomposed into two parts: $u = u_1 + u_2$ where u_1 is measured with the TV norm and u_2 is measured using a higher order norm. Thus, given an observed noisy image f, the CL model is formulated as an energy minimization problem:

$$\inf_{u_1,u_2} \left\{ E(u) = \int_\Omega |\nabla u_1| + \alpha \int_\Omega |\partial^2 u_2| + \lambda \int_\Omega (f - u_1 - u_2)^2 d\mathbf{x} \right\}. \tag{2}$$

The minimization of this energy has the requirement that the discontinuous component of the image be assigned to the u_1 component while regions of moderate slopes are allotted to the u_2 component. The allocation of regions to u_2 is of small cost since regions of moderate but constant gradients measure zero for the higher order norm. In the 1-d examples presented in [9], staircasing is reduced to a remarkable degree .

Another approach to reducing staircasing in TV reconstructions is introduced in the following model by Blomgren, Mulet, Chan, and Wong [5]:

$$\inf_{u}\left\{E(u)=\int_{\Omega}|\nabla u|^{Q(|\nabla u|)}+\lambda(f-u)^2 d\mathbf{x}\right\}. \tag{3}$$

Here, the authors choose the function $Q(\xi):\mathbb{R}\to\mathbb{R}$ to monotonically decrease from 2 when $\xi=0$, to 1 as ξ tends to infinity. Thus, the functional (3) is designed to be more convex in regions of moderate gradient (away from discontinuities) and behave like the standard ROF model near discontinuities, hence reducing staircasing.

A variant of the CL model (2) is introduced by Chan, Esedoglu, and Park (CEP) [11] for fast staircase reduction in denoising problems. Their model, which is referred to as the CEP–L^2 model (for the L^2 norm squared of the component $v=f-u_1-u_2$), has the following formulation:

$$\inf_{u_1,u_2}\left\{\int_{\Omega}|\nabla u_1|+\frac{\alpha}{2}\int_{\Omega}|\Delta u_2|^2+\frac{\lambda}{2}\int_{\Omega}(f-u_1-u_2)^2\,d\mathbf{x}\right\}. \tag{4}$$

The main idea here, is to approximate the term $\int_\Omega|\partial^2 u_2|$ found in the original CL model (2), by the term $\int_\Omega|\Delta u_2|^2$. The authors show that this approximation allows for fast solvers for the u_2 component while successfully decreasing staircasing.

In addition to applications in image denoising, the TV norm has also been utilized in many of the current texture decomposition models, particularly those based on the Meyer norms, to model the structural (geometric) part of an image. In the fundamental work [17], Meyer introduces the notion that image denoising can be thought of as image decomposition for the application of texture extraction. He then introduces a variant of the popular ROF model based on a space called the G space for this particular purpose. Meyer's idea is to replace the L^2 norm in the ROF model with a weaker norm that better captures very oscillatory features construed as texture. Thus, the G space is essentially the dual space to the space of functions of *bounded variation* (BV) and is defined as the following:

$$G=\{v\mid v=\partial_x g_1(x,y)+\partial_y g_2(x,y),\ g_1,g_2\in L^\infty(\Omega)\} \tag{5}$$

induced by the norm:

$$\|v\|_*=\inf_{\mathbf{g}=(g_1,g_2)}\left\{\|\sqrt{{g_1}^2+{g_2}^2}\|_{L^\infty}\mid v=\partial_x g_1+\partial_y g_2\right\}. \tag{6}$$

Given a function f defined on Ω, Meyer's decomposition model then follows as:

$$\inf_{u}\left\{E(u)=\int_{\Omega}|\nabla u|+\lambda\|v\|_*,\ f=u+v\right\}. \tag{7}$$

In this model, the u component represents the structure or geometric part of the image while the oscillatory component v represents the texture part, thus, yielding the so called $u+v$ decomposition: $f=u+v$. It is shown numerically, by the authors in [22, 18], that the $*$ norm indeed captures oscillatory patterns (texture) better than the standard ROF model. The first practical algorithm to approximate Meyer's G model (7) is found in the work by Vese and Osher [22].

Although TV regularization has been a popular choice for modelling structural components of an image, the staircasing caveat, as in the denoising case, also occurs in the context of texture extraction.

Some very recent efforts have been made to alleviate this particular attribute of the TV norm in conjunction with decomposition models based on the the Meyer norms. In the work by Chan, Esedoglu, and Park (CEP) [11], the authors consider incorporating the energy proposed by Chambolle and Lions (2) into texture decomposition models based on the Meyer norms [17] to reduce staircasing in the structural components of the image decomposition. Thus, the general proposed model in [11] is based on the original model of Meyer and has the following formulation:

$$\inf_{u_1,u_2}\left\{\int_\Omega |\nabla u_1| + \alpha\int_\Omega \left|\partial^2 u_2\right| + \lambda\|v\|_*,\ f = u_1+u_2+v\right\}. \tag{8}$$

To allow for fast solvers for the u_2 component, the authors then introduce a variant of the the CL energy, where the quantity $\int|\Delta u_2|^2 d\mathbf{x}$ is used to approximate the term $\int|\partial^2 u_2|$ in the original CL model. This proposed general model is called the CEP-G model for Meyer's G norm and has the following formulation:

$$\inf_{u_1,u_2}\left\{\int_\Omega |\nabla u_1| + \frac{\alpha}{2}\int_\Omega |\Delta u_2|^2 + \lambda\|v\|_*,\ f = u_1+u_2+v\right\}. \tag{9}$$

The CEP–G model (9), in practice, is difficult to implement due to the intrinsic nature of the $*$ norm. However, the authors adapt the previous approaches of approximating Meyer's model in [18, 1, 2] to the approximation of the above model (9) resulting in the CEP models and approximations. In this setting, the approximation to the CEP-G model, called the CEP-G approximation, is based on the approach in [1] and has the following formulation:

$$\inf_{\{(u,v)\in\Omega\times\Omega,\ u=u_1+u_2\}}\left\{\int_\Omega |\nabla u_1| + \frac{\alpha}{2}\int_\Omega |\Delta u_2|^2 + J^*\left(\frac{v}{\mu}\right) + \frac{1}{2\lambda}\int_\Omega (f-u_1-u_2-v)^2\, d\mathbf{x}\right\}. \tag{10}$$

Here, the terms $\int_\Omega|\nabla u_1|+\frac{\alpha}{2}\int_\Omega|\Delta u_2|^2$ simultaneously model the structural (geometric) part of the image while reducing staircasing. The term $J^*\left(\frac{v}{\mu}\right) = \chi_{\{v\ |\ \|v\|_G\le\mu\}}$ ensures that the texture component v lies in the G space with $\|v\|_G \le \mu$, and the quantity $\frac{1}{2\lambda}\int_\Omega (f-u_1-u_2-v)^2$ secures the decomposition $f = u_1+u_2+v$ for small λ. Now, as $\lambda \longrightarrow 0$, the authors state that by using similar arguments to those in [1], one can show that minimizing the energy in (10) yields a solution to the CEP–G model (9).

A staircase reducing texture extraction model involving a negative Sobolev norm is also introduced by the authors of [11]. This model, called the CEP–H^{-1} model, is based on the model by Osher, Sole, and Vese (OSV) [18] utilizing the H^{-1} norm. The OSV model can be thought of as both a variant and approximation to the original model by Meyer (7) and has proven to be useful in texture extraction problems. The CEP–H^{-1} model extends the OSV model to staircase reducing texture extraction problems and has the following formulation:

$$\inf_{u_1,u_2}\left\{\int_\Omega |\nabla u_1| + \alpha\int_\Omega |\Delta u_2|^2 + \frac{1}{2\lambda}\int_\Omega \left|\nabla\Delta^{-1}(f-u_1-u_2)\right|^2 d\mathbf{x}\right\}. \tag{11}$$

The authors show that staircase reduction can be obtained both naturally and efficiently while not affecting the texture removal properties of the negative norm.

The authors of [11] also replace the G norm in model (9) with the E norm, E denoting the space $B^\infty_{-1,\infty}$, the dual to the standard Besov space $B^1_{1,1}$, to obtain the following CEP–E model:

$$\inf_{u_1,u_2}\left\{\int_\Omega |\nabla u_1| + \frac{\alpha}{2}\int_\Omega |\Delta u_2|^2 + \lambda\|v\|_E,\ f = u_1+u_2+v\right\}. \tag{12}$$

Again, as in the case of the CEP–G model, the E norm is difficult to implement in practice, however, one may consider the following CEP–E approximation:

$$\inf_{\{(u,v)\in\Omega\times\Omega,\ u=u_1+u_2\}} \left\{ \int_\Omega |\nabla u_1| + \frac{\alpha}{2}\int_\Omega |\Delta u_2|^2 + B^*\left(\frac{v}{\gamma}\right) + \frac{1}{2\lambda}\int_\Omega (f-u_1-u_2-v)^2\, d\mathbf{x} \right\}. \tag{13}$$

This approximation is a staircase reducing variant of the approximation in [2] and the term $B^*\left(\frac{v}{\gamma}\right) = \chi_{\{v\ |\ \|v\|_E\leq\gamma\}}$ enforces the texture component v to lie in the E space with norm $\|v\|_E \leq \gamma$. The authors also state that, by using similar arguments as in [1], one can also show that minimizing the energy in (13) yields a solution to the CEP–E model (12). As demonstrated in [2], the E norm has proven to be a good candidate for denoising textured images.

In addition to the staircase reducing $u+v$ (structure and texture models), the authors of [11] also introduce a variant to the $u+v+w$ (structure+texture+noise) model introduced in [2] for staircase reducing $u+v+w$ decompositions. This model, called the CEP-UVW model has the following formulation:

$$\inf_{u_1,u_2,v,w} \left\{ \int_\Omega \left\{ |\nabla u_1| + \frac{\alpha}{2}|\Delta u_2|^2 \right\} + J^*\left(\frac{v}{\mu}\right) + B^*\left(\frac{w}{\delta}\right) + \frac{1}{2\lambda}\int_\Omega (f-u_1-u_2-v-w)^2 d\mathbf{x} \right\}, \tag{14}$$

where $J^*\left(\frac{v}{\mu}\right)$ and $B^*\left(\frac{w}{\delta}\right)$ are defined in exactly the same manner as in the approximations (10) and (13) respectively.

The main contribution of this paper is the introduction of the 4-th order energy

$$\|\Delta u_2\|_1 = \int_\Omega |\Delta u_2| \tag{15}$$

into the image restoration and texture extraction models proposed by Chan, Esedoglu, and Park [11] leading to new staircase reducing models in image processing along with novel high 4-th order dual methods to obtain the corresponding solutions. The advantage of the proposed non-smooth energy (15) over the energy used in the original CEP models is the ability to preserve discontinuities in the second derivative manifesting themselves as kinks or ridges in an image or signal. In contrast, the energy utilized in the original CEP models $\|\Delta u_2\|_2^2$, while being differentiable as well as allowing for fast solvers, cannot preserve such discontinuities; an example of this property can be seen in Figure 2. The 4-th order dual method is novel since existing dual methods have primarily been used in conjunction with second order energies like those found in the ROF model, see [7, 2]. To the best of the combined authors' knowledge, the method in this paper is the first instance of a high order dual method in image processing. Convergence proofs for the proposed dual method will also be provided in the context of the new CEP models and we claim that the method is faster and more stable than the popular artificial time marching algorithms so frequently used on such models. Additionally, the new method solves the non-differentiability issue of the proposed energy (15) at zero. When the primal problem of minimizing the energy $\|\Delta u_2\|_1$ is considered, one must regularize the energy with a small β parameter:

$$\int_\Omega \sqrt{(\Delta u_2)^2 + \beta^2}. \tag{16}$$

Unfortunately, when employing artificial time marching methods for the minimization of the above energy (16), when combined with appropriate data fidelity terms, the resulting minimization problem becomes stiff when β is chosen small. Larger parameters of β tend to smear out discontinuities. When utilizing a dual method, the non-smooth issue of the energy (15) is bypassed and the small β regularization parameter may be eliminated.

Some related works include, a decomposition model based on the anisotropic ROF model seen in [15] while two others based on an L^1 fidelity term can be found in [10, 3]. Two multiscale decompositions based on the TV model are introduced in [14, 21] while a simultaneous structure and texture image inpainting model is found in [4]. A staircase reducing texture extraction and restoration model that combines the energy introduced by Blomgren, Mulet, Chan, and Wong (3) with a negative norm is introduced in the work by Levine et al. [16].

2 The CEP2–L^2 Denoising Model and a Fourth Order Dual Method

The proposed CEP–L^2 staircase reducing image denoising model is a variant of the models by Chambolle and Lions (2) and Chan, Esedoglu, and Park (4) and has the following formulation:

$$\inf_{u_1,u_2}\left\{\int_\Omega |\nabla u_1| + \alpha\int_\Omega |\Delta u_2| + \frac{1}{2\lambda}\int_\Omega (f-u_1-u_2)^2 d\mathbf{x}\right\}. \tag{17}$$

This model, like its predecessors, can also be interpreted as a decomposition model where a given image f is split as $f = u_1 + u_2 + v$. Here, u_1, u_2, and v are the discontinuous, piecewise smooth, and noise components respectively.

One way of minimizing the energy (17) is by solving the coupled problems:

for u_1 fixed, solve for u_2:

$$\inf_{u_2} \alpha\int_\Omega |\Delta u_2| + \frac{1}{2\lambda}\int_\Omega (f-u_1-u_2)^2 d\mathbf{x} \tag{18}$$

for u_2 fixed, solve for u_1:

$$\inf_{u_1} \int_\Omega |\nabla u_1| + \frac{1}{2\lambda}\int_\Omega (f-u_1-u_2)^2 d\mathbf{x}. \tag{19}$$

Equation (18), is usually solved by time marching the fourth order non-linear Euler-Lagrange equation obtained from this energy. Unfortunately, such a method has some potential caveats due to the, non-differentiability of the energy, the nonlinear nature of the corresponding Euler-Lagrange equation, and the CFL restrictions from the high (4-th) order. Alternatively, the problem of solving for u_2 in equation (18) can be set in the primal-dual formulation:

$$\inf_{u_2}\sup_{\xi}\left\{\alpha\int_\Omega u_2\Delta\xi d\mathbf{x} + \frac{1}{2\lambda}\int_\Omega (f-u_1-u_2)^2 d\mathbf{x} \mid \xi\in C_c^2(\Omega;\mathbb{R}),\ -1\le\xi\le 1\right\} \tag{20}$$

where ξ is a scalar valued function, $\xi:\Omega\to\Omega$. The above equation (20) is convex in u_2 and concave (linear) in ξ, thus, we may swap the inf and sup in (20) to yield:

$$\sup_{\xi}\inf_{u_2}\left\{\alpha\int_\Omega u_2\Delta\xi d\mathbf{x} + \frac{1}{2\lambda}\int_\Omega (f-u_1-u_2)^2 d\mathbf{x} \mid \xi\in C_c^2(\Omega;\mathbb{R}),\ -1\le\xi\le 1\right\}. \tag{21}$$

For each fixed ξ, we consider the inner minimization in (21):

$$\inf_{u_2}\left\{G(u_2) = \alpha\int_\Omega u_2\Delta\xi d\mathbf{x} + \frac{1}{2\lambda}\int_\Omega (f-u_1-u_2)^2 d\mathbf{x} \mid \xi\in C_c^2(\Omega;\mathbb{R}),\ -1\le\xi\le 1\right\}. \tag{22}$$

Here, for each ξ, a minimizer u_2 of (22) has the form $u_2 = f - u_1 - \alpha\lambda\Delta\xi$. Substituting this expression for u_2 back into (21) and setting $\sup\{G(\cdot)\} = -\inf\{-G(\cdot)\}$ reformulates problem (22) into:

$$-\inf_{\xi} \alpha \left\{ \int_{\Omega} \left(\frac{\alpha\lambda}{2} (\Delta\xi)^2 - (f - u_1)\Delta\xi \right) d\mathbf{x} \mid \xi \in C_c^2(\Omega; \mathbb{R}),\ -1 \le \xi \le 1 \right\}. \tag{23}$$

Since we are concerned only with $\Delta\xi$, we may rewrite the above minimization (23) as the following full dual problem:

$$\inf_{\xi} \left\{ \int_{\Omega} \left(\frac{\alpha\lambda}{2} (\Delta\xi)^2 - (f - u_1)\Delta\xi \right) d\mathbf{x} \mid \xi \in C_c^2(\Omega; \mathbb{R}),\ -1 \le \xi \le 1 \right\}. \tag{24}$$

In the discrete setting, minimizing the above equation (24) amounts to solving the following constrained optimization problem with inequality constraints:

$$\min_{p, |p| \le 1} \left\{ \int_{\Omega} \left(\frac{\alpha\lambda}{2} (\Delta p)^2 - (f - u_1)\Delta p \right) d\mathbf{x} \right\}. \tag{25}$$

The optimality condition for the above problem (25) reads:

$$\left(\alpha\lambda\Delta^2 p - \Delta(f - u_1)\right)_{i,j} + \alpha_{i,j} p_{i,j} = 0 \tag{26}$$

where the $\alpha_{i,j}$'s are the Lagrange Multipliers, and by complementary slackness, either $\alpha_{i,j} = 0$ (where $\Delta(\alpha\lambda\Delta^2 p + f - u_1)_{i,j}$ is also 0) and $|p_{i,j}| < 1$ or $\alpha_{i,j} > 0$ and $|p_{i,j}| = 1$. Here, we would like to take the time to point out that the approach of solving a similar equation to (26) arising from the ROF model in the dual framework was pursued by the authors in [6, 12]. Using the key observation and essential contribution in [7], we see that in either of the cases, the Lagrange multipliers are:

$$\alpha_{i,j} = \left|\alpha\lambda\Delta^2 p - \Delta(f - u_1)\right|_{i,j}. \tag{27}$$

Setting $A(p) = \Delta^2 p - \Delta\left(\frac{f - u_1}{\alpha\lambda}\right)$ implies that equation (26) reduces to:

$$A(p)_{i,j} + |A(p)_{i,j}| p_{i,j} = 0 \tag{28}$$

which can be solved by a semi-implicit gradient descent (fixed point) iteration introduced in [7]:

$$p^0 = 0; \quad p_{i,j}^{n+1} = p_{i,j}^n - \tau\left(A_{i,j}^n + |A_{i,j}^n| p_{i,j}^{n+1}\right). \tag{29}$$

The scheme (29) then simplifies to the explicit iteration scheme:

$$p^0 = 0; \quad p_{i,j}^{n+1} = \frac{p_{i,j}^n - \tau A_{i,j}^n}{1 + \tau |A_{i,j}^n|} \tag{30}$$

where $A_{i,j}^n = \Delta^2 p_{i,j}^n - \Delta\left(\frac{f-u_1}{\alpha\lambda}\right)_{i,j}$ and $u_2^n = f - u_1 - \alpha\lambda\Delta p^n \longrightarrow \tilde{u_2}$ as $n \longrightarrow \infty$, with $\tilde{u_2}$ a solution of (18).

Before stating the convergence result associated to the above method (30), we first note that the constrained optimization problem (25) is equivalent to the following:

$$\min_{p, |p| \le 1} \left\{ \int_{\Omega} \left(\Delta p - \frac{f - u_1}{\alpha\lambda} \right)^2 d\mathbf{x} \right\}. \tag{31}$$

Theorem 2.1 Let $\tau < 1/64$. Then, $v^n = \Delta p^n$ converges to the solution of the minimization problem (25) as $n \longrightarrow \infty$.

Proof. Fix $n \geq 0$ and set $\eta = \frac{p^{n+1}-p^n}{\tau}$. Then,

$$\begin{aligned} \|\Delta p^{n+1} - (f-u_1)/\beta\|^2 &= \|\Delta p^n - (f-u_1)/\beta\|^2 + 2\tau \langle \Delta\eta, \Delta p^n - (f-u_1)/\beta\rangle + \tau^2\|\Delta\eta\|^2 \\ &\leq \|\Delta p^n - (f-u_1)/\beta\|^2 + \tau\left(2\langle \eta, \Delta(\Delta p^n - (f-u_1)/\beta)\rangle + \kappa^2\tau\|\eta\|^2\right) \end{aligned}$$

where $\beta = \alpha\lambda$, $\|\eta\|^2 = \langle \eta, \eta\rangle$, and κ denotes the norm of the operator Δ to be computed shortly. Let $A^n_{i,j}$ be defined by $A^n_{i,j} = \Delta\left(\Delta p^n - (f-u_1)/\beta\right)$, so that

$$2\langle \eta, A^n\rangle + \kappa^2\tau\|\eta\|^2 = \sum_{i,j=1}^{N} 2\eta_{i,j}A^n_{i,j} + \kappa^2\tau|\eta_{i,j}|^2, \tag{32}$$

with the quantity $\eta_{i,j} = -A^n_{i,j} - \varrho_{i,j}$ where $\varrho_{i,j} = |A^n_{i,j}|p^{n+1}_{i,j}$. Therefore, for each i, j

$$2\eta_{i,j}A^n_{i,j} + \kappa^2\tau|\eta_{i,j}|^2 = \left(\kappa^2\tau - 1\right)|\eta_{i,j}|^2 + |\varrho_{i,j}|^2 - |A^n_{i,j}|^2. \tag{33}$$

Now, $|p^{n+1}_{i,j}| \leq 1$ implies that $|\varrho_{i,j}| \leq |A^n_{i,j}|$. Thus, $|\varrho_{i,j}|^2 \leq |A^n_{i,j}|^2$. Hence, if $\left(\kappa^2\tau - 1\right) \leq 0$, i.e. $\tau \leq 1/\kappa^2$, the quantity $\|\Delta p^n - (f-u_1)/\beta\|^2$ is decreasing as n increases as long as $\eta \neq 0$. If $\eta = 0$, then $p^{n+1} = p^n$. More analysis also shows that the energy still decreases in the case when $\kappa^2\tau = 1$.

Now, set $L = \lim_{n\to\infty}\|\Delta p^n - (f-u_1)/\beta\|$ and let $\{p^{n_q}\}$ be a convergent subsequence with limit $\tilde{p}$. If we let $\hat{p} = \lim_{n_q\to\infty} p^{n_q+1}$ then, we have

$$\hat{p}_{i,j} = \frac{\tilde{p}_{i,j} - \tau\Delta\left(\Delta\tilde{p} - (f-u_1)/\beta\right)_{i,j}}{1 + \tau\left|\Delta\left(\Delta\tilde{p} - (f-u_1)/\beta\right)_{i,j}\right|}. \tag{34}$$

Repeating the calculations at the beginning of the proof and taking limits yields

$$\|\Delta\hat{p} - (f-u_1)/\beta\|^2 \leq \|\Delta\tilde{p} - (f-u_1)/\beta\|^2 + \tau\left(\kappa^2\tau - 1\right)\|\tilde{\eta}\|^2. \tag{35}$$

where $\tilde{\eta} = \frac{\hat{p}-\tilde{p}}{\tau}$. Now, $L = \|\Delta\tilde{p} - (f-u_1)/\beta\| = \|\Delta\hat{p} - (f-u_1)/\beta\|$ implying that $\tilde{\eta}_{i,j} = \frac{\hat{p}_{i,j}-\tilde{p}_{i,j}}{\tau} = 0$ for every i, j. Therefore, $\tilde{p} = \hat{p}$ and

$$\Delta\left(\Delta\tilde{p} - (f-u_1)/\beta\right)_{i,j} + \left|\Delta\left(\Delta\tilde{p} - (f-u_1)/\beta\right)_{i,j}\right|\tilde{p}_{i,j} = 0 \tag{36}$$

the optimality equation for a solution that minimizes problem (25). Therefore, $\Delta\tilde{p}$ is the solution to problem (25). Since this solution is unique, the complete sequence $\{\Delta p^n\}$ converges to the solution of (25). Thus, the theorem is proved if we can show that $\kappa^2 \leq 64$.

By definition, $\kappa = \sup_{\|p\|\leq 1}\|\Delta P\|$. Using the standard zero boundary conditions on $p_{i,j}$, we have:

$$\begin{aligned} \|\Delta p\|^2 &\leq \sum_{i,j}\left(p_{i+1,j} - 2p_{i,j} + p_{i-1,j} + p_{i,j+1} - 2p_{i,j} + p_{i,j-1}\right)^2 \\ &\leq \sum_{i,j} 2\left(p_{i+1,j} + p_{i-1,j} + p_{i,j+1} + p_{i,j-1}\right)^2 + 8\left(p_{i,j} + p_{i,j}\right)^2 \\ &\leq \sum_{i,j} 8\left\{(p_{i+1,j})^2 + (p_{i-1,j})^2 + (p_{i,j+1})^2 + (p_{i,j-1})^2\right\} + 16\left\{(p_{i,j})^2 + (p_{i,j})^2\right\} \\ &\leq 64\|p\|^2. \end{aligned}$$

Thus, $\kappa^2 \leq 64$. $\Diamond$

The discontinuous component u_1 can be obtained by solving equation (19), which is essentially a slight variation to the ROF model. To solve (19), one can employ either artificial time marching methods, or, keeping with the theme of this paper, a dual method like those introduced in [6, 7, 12]. We outline a method that is a slight variation of the dual method introduced in [7] where, for u_2 fixed, the primal-dual formulation of problem (19)

$$\inf_{u_1} \sup_{\boldsymbol{\xi}} \left\{ \int_\Omega u_1 \mathrm{div}(\boldsymbol{\xi}) + \frac{1}{2\lambda} \int_\Omega (f - u_1 - u_2)^2 \, d\mathbf{x} \;\mid\; \boldsymbol{\xi} \in C_c^1(\Omega; \mathbb{R}^2),\ |\boldsymbol{\xi}| \leq 1 \right\}, \tag{37}$$

in the discrete setting, can be reformulated as the following full dual constrained optimization problem with inequality constraints

$$\min_{\boldsymbol{p}, |\boldsymbol{p}| \leq 1} \left\{ \int_\Omega (\lambda \mathrm{div}(\boldsymbol{p}) - (f - u_2))^2 \right\}, \tag{38}$$

where $\boldsymbol{\xi}$ and $\boldsymbol{p}$ are now vector valued functions, $\boldsymbol{\xi} : \Omega \to \Omega \times \Omega$. In this setting, the above problem (38) has optimality conditions that read:

$$-\nabla \left(\lambda \mathrm{div}(\boldsymbol{p}) - (f - u_2) \right)_{i,j} + \alpha_{i,j} \boldsymbol{p}_{i,j} = \mathbf{0}$$

where $\alpha_{i,j}$ are the Lagrange multipliers and by complementary slackness, either $\alpha_{i,j} = 0$ and $|\boldsymbol{p}_{i,j}| < 1$ or $\alpha_{i,j} > 0$ and $|\boldsymbol{p}_{i,j}| = 1$. Once again, the key observation in [7] implies that the Lagrange multipliers $\alpha_{i,j}$ reduce to $\alpha_{i,j} = \left| \nabla \left(\lambda \mathrm{div}(\boldsymbol{p}) - (f - u_2) \right)_{i,j} \right|$. Thus, the optimality equation reduces to:

$$-\boldsymbol{A}(\boldsymbol{p})_{i,j} + |\boldsymbol{A}(\boldsymbol{p})_{i,j}| \boldsymbol{p}_{i,j} = \mathbf{0}$$

where $\boldsymbol{A}(\boldsymbol{p})_{i,j} = \nabla \left(\mathrm{div}(\boldsymbol{p}) - \frac{f - u_2}{\lambda} \right)_{i,j}$. Again, this equation can be solved by the gradient descent (fixed point) iteration scheme introduced in [7]:

$$\boldsymbol{p}^0 = \mathbf{0}, \quad \boldsymbol{p}_{i,j}^{n+1} = \frac{\boldsymbol{p}_{i,j}^n + \tau \boldsymbol{A}_{i,j}^n}{1 + |\boldsymbol{A}_{i,j}^n|}$$

where $\boldsymbol{A}_{i,j}^n = \nabla \left(\mathrm{div}(\boldsymbol{p}^n) - \frac{f - u_2}{\lambda} \right)_{i,j}$. It is proven by the author in [7] that for the ROF model (i.e. in the case when $u_2 = 0$), that for $\tau \leq \frac{1}{8}$, $u_1^n = f - u_2 - \lambda \mathrm{div}(\boldsymbol{p}^n) \longrightarrow \tilde{u_1}$ as $n \longrightarrow \infty$, where $\tilde{u_1}$ is a solution to (19).

3 The CEP2–H^{-1} Model and a Fourth Order Dual Formulation

The proposed staircase reducing texture extraction model involving the H^{-1} norm is called the *CEP2–H^{-1}* model and has the following formulation:

$$\inf_{u_1, u_2} \left\{ \int_\Omega |\nabla u_1| + \alpha \int_\Omega |\Delta u_2| + \frac{1}{2\lambda} \int_\Omega |\nabla \Delta^{-1} (f - u_1 - u_2)|^2 \right\}. \tag{39}$$

This image decomposition model splits a given image f into $f = u + v$ where $u = u_1 + u_2$ and $v = f - u_1 - u_2$. Here, u and v represent the structure (geometric features) and texture (oscillatory features) components respectively. The energy $\|\Delta u_2\|_1$ reduces staircasing in the structure component $u = u_1 + u_2$ where u_1 and u_2 represent the discontinuous and piecewise smooth parts of u respectively. The proposed model is motivated by the CEP–H^{-1} model of [11]. We will adapt the same techniques applied to the CEP2–L^2 model in the previous section to the proposed image decomposition model (39). Moreover, demonstrations of the proposed model to the problem of staircase reduction in texture extraction will follow.

One way of minimizing the energy of the proposed model (39) is by minimizing the coupled energies:

for u_1 fixed, solve for u_2:

$$\inf_{u_2} \left\{ \alpha \int_\Omega |\Delta u_2| d\mathbf{x} + \frac{1}{2\lambda} \int_\Omega |\nabla \Delta^{-1} (f - u_1 - u_2)|^2 d\mathbf{x} \right\}, \tag{40}$$

for u_2 fixed, solve for u_1:

$$\inf_{u_1} \left\{ \int_\Omega |\nabla u_1| + \frac{1}{2\lambda} \int_\Omega |\nabla \Delta^{-1} (f - u_1 - u_2)|^2 d\mathbf{x} \right\}. \tag{41}$$

To solve for the u_2 component, we consider a high order dual formulation of the above problem (40):

for u_1 fixed, solve:

$$\inf_{u_2} \sup_{\xi} \left\{ \alpha \int_\Omega u_2 \Delta\xi d\mathbf{x} + \frac{1}{2\lambda} \int_\Omega |\nabla \Delta^{-1} (f - u_1 - u_2)|^2 d\mathbf{x} \ \middle| \ \xi \in C_c^2(\Omega),\ -1 \leq \xi \leq 1 \right\} \tag{42}$$

where $\xi : \Omega \to \Omega$ is a scalar valued function. The above primal-dual equation (42) is convex in u_2 and concave (linear) in ξ, thus, we may swap the sup and inf to yield:

$$\sup_{\xi} \inf_{u_2} \left\{ \alpha \int_\Omega u_2 \Delta\xi d\mathbf{x} + \frac{1}{2\lambda} \int_\Omega |\nabla \Delta^{-1} (f - u_1 - u_2)|^2 d\mathbf{x} \ \middle| \ \xi \in C_c^2(\Omega),\ -1 \leq \xi \leq 1 \right\}. \tag{43}$$

Minimizing the inner quantity of (43)

$$\inf_{u_2} \left\{ G(u_2) = \alpha \int_\Omega u_2 \Delta\xi d\mathbf{x} + \frac{1}{2\lambda} \int_\Omega |\nabla \Delta^{-1} (f - u_1 - u_2)|^2 d\mathbf{x} \right\} \tag{44}$$

with respect to u_2, for each fixed ξ, admits $u_2 = f - u_1 + \alpha\lambda\Delta^2\xi$. Substituting this expression for u_2 back into equation (43), integrating by parts, and using the fact that $\sup\{G(\cdot)\} = -\inf\{-G(\cdot)\}$, reduces problem (43) to the following full dual minimization problem:

$$-\inf_{\xi} \left\{ \int_\Omega \frac{\alpha^2\lambda}{2} |\nabla (\Delta\xi)|^2 - \alpha(f - u_1)\Delta\xi d\mathbf{x} \ \middle| \ \xi \in C_c^2(\Omega),\ -1 \leq \xi \leq 1 \right\}. \tag{45}$$

Since we are only concerned with $\Delta\xi$, the above problem (45) may be reformulated as the following minimization problem

$$\inf_{\xi} \left\{ \int_\Omega \frac{\beta}{2} |\nabla (\Delta\xi)|^2 - (f - u_1)\Delta\xi d\mathbf{x} \ \middle| \ \xi \in C_c^2(\Omega),\ -1 \leq \xi \leq 1 \right\} \tag{46}$$

where $\beta = \alpha\lambda$. In the discrete setting, the above problem (46) amounts to solving the constrained optimization problem with inequality constraints:

$$\min_{p, |p| \leq 1} \left\{ \int_\Omega \frac{\beta}{2} |\nabla (\Delta p)|^2 - (f - u_1) \Delta p d\mathbf{x} \right\}. \tag{47}$$

Given the Lagrange Multipliers connected to the above problem (47), the optimality conditions read:

$$-\Delta(\beta\Delta^2 p + f - u_1)_{i,j} + \alpha_{i,j} p_{i,j} = 0 \tag{48}$$

where by complementary slackness, either $\alpha_{i,j} = 0$ (where $-\Delta(\beta\Delta^2\xi + f - u_1)_{i,j}$ is also 0) and $|p_{i,j}| < 1$ or $\alpha_{i,j} > 0$ and $|p_{i,j}| = 1$. Again, we would like to point out that the approach of solving a similar equation to (48) arising from the ROF model in the dual framework was pursued in [6, 12]. Once again, using the observation and essential contribution in [7], we see that in either case, the Lagrange multipliers are:

$$\alpha_{i,j} = |\Delta(\beta\Delta^2 p + f - u_1)_{i,j}|. \tag{49}$$

Thus, the optimality equation (48) reduces to

$$-A(p)_{i,j} + |A(p)_{i,j}| p_{i,j} = 0 \tag{50}$$

where $A(p)_{i,j} = \Delta(\Delta^2 p + (f - u_1)/\beta)_{i,j}$. This equation can be solved by the semi-implicit gradient descent (fixed point) iteration scheme introduced in [7]:

$$p^0 = 0, \quad p_{i,j}^{n+1} = \frac{p_{i,j}^n + \tau A_{i,j}^n}{1 + \tau |A_{i,j}^n|} \tag{51}$$

where $A_{i,j}^n = \Delta(\Delta^2 p^n + (f - u_1)/\beta)_{i,j}$. It will be shown shortly, that Δp^n converges to the solution of (47) for τ small enough; hence, $u_2^n = f - u_1 + \beta\Delta^2 p^n \longrightarrow \tilde{u_2}$ as $n \longrightarrow \infty$, where $\tilde{u_2}$ is a solution to the original minimization problem (42).

Before stating the convergence result of the proposed method (51), we remark that the above minimization problem (47) is equivalent to the following:

$$\min_p \left\{ \int_\Omega |\nabla (\Delta p)|^2 - 2(f - u_1)/\beta \Delta p d\mathbf{x} \;\middle|\; p \in \Omega, \; -1 \leq p \leq 1 \right\}. \tag{52}$$

Theorem 3.1 Let $\tau < 1/512$. Then, $v^n = \Delta p^n$ converges to the solution of the minimization problem (47) as $n \longrightarrow \infty$.

Proof. Fix $n \geq 0$ and set $\eta = \frac{p^{n+1} - p^n}{\tau}$. Then,

$$\begin{aligned}
\|\nabla\Delta p^{n+1}\|^2 - \frac{2}{\beta}\left\langle f - u_1, \Delta p^{n+1}\right\rangle &\leq \|\nabla\Delta p^n\|^2 - \frac{2}{\beta}\langle f - u_1, \Delta p^n\rangle \\
&+ \tau\left(2\langle\nabla\Delta p^n, \nabla\Delta\eta\rangle - \frac{2}{\beta}\langle f - u_1, \Delta\eta\rangle + \tau\kappa^2\|\eta\|^2\right) \\
&= \|\nabla\Delta p^n\|^2 - \frac{2}{\beta}\langle f - u_1, \Delta p^n\rangle \\
&+ \tau\left(-2\left\langle\Delta\left(\Delta^2 p^n + (f - u_1)/\beta\right), \eta\right\rangle + \tau\kappa^2\|\eta\|^2\right).
\end{aligned}$$

where $\|\eta\|^2 = \langle \eta, \eta \rangle$ and κ denotes the norm of the operator $\nabla\Delta$ to be computed shortly. Let $A^n_{i,j} = \Delta\left(\Delta^2 p^n + \frac{(f-u_1)}{\beta}\right)$. Now,

$$-2\langle \eta, A^n \rangle + \kappa^2\tau\|\eta\|^2 = \sum_{i,j=1}^{N} -2\eta_{i,j}A^n_{i,j} + \kappa^2\tau|\eta_{i,j}|^2 \tag{53}$$

and the quantity $\eta_{i,j} = A^n_{i,j} - \varrho_{i,j}$ with $\varrho_{i,j} = |A^n_{i,j}|p^{n+1}_{i,j}$. Therefore, for each i, j

$$-2\eta_{i,j}A^n_{i,j} + \kappa^2\tau|\eta_{i,j}|^2 = \left(\tau\kappa^2 - 1\right)|\eta_{i,j}|^2 + |\varrho_{i,j}|^2 - |A^n_{i,j}|^2. \tag{54}$$

Now, $|p^{n+1}_{i,j}| \leq 1$ implies that $|\varrho_{i,j}| \leq |A^n_{i,j}|$. Thus, $|\varrho_{i,j}|^2 \leq |A^n_{i,j}|^2$. Hence, if $\left(\tau\kappa^2 - 1\right) \leq 0$, i.e. $\tau \leq 1/\kappa^2$, the quantity

$$\|\nabla\Delta p^n\|^2 - \frac{2}{\beta}\langle f - u_1, \Delta p^n \rangle$$

is decreasing as n increases as long as $\eta \neq 0$. If $\eta = 0$, then $p^{n+1} = p^n$. More analysis also shows that the energy still decreases in the case when $\kappa^2\tau = 1$.

Now, set $L = \lim_{n\to\infty}\left\{\|\nabla\Delta p^n\|^2 - \frac{2}{\beta}\langle f - u_1, \Delta p^n\rangle\right\}$, let $\{p^{n_q}\}$ be a convergent subsequence with limit $\tilde{p}$, and let $\hat{p} = \lim_{n_q\to\infty} p^{n_q+1}$. Then, we have

$$\hat{p}_{i,j} = \frac{\tilde{p}_{i,j} + \tau\Delta(\Delta^2\tilde{p} + (f-u_1)/\beta)_{i,j}}{1 + \tau\left|\Delta(\Delta^2\tilde{p} + (f-u_1)/\beta)_{i,j}\right|}. \tag{55}$$

Repeating the previous calculations and taking limits yields

$$\|\nabla\Delta\hat{p}\|^2 - \frac{2}{\beta}\langle f - u_1, \Delta\hat{p}\rangle \quad\leq\quad \|\nabla\Delta\tilde{p}\|^2 - \frac{2}{\beta}\langle f - u_1, \Delta\tilde{p}\rangle \;+\; \tau(\tau\kappa^2 - 1)\kappa^2\|\tilde{\eta}\|^2 \tag{56}$$

where $\tilde{\eta} = \frac{\hat{p}-\tilde{p}}{\tau}$. Now, $L = \left\{\|\nabla\Delta\hat{p}\|^2 - \frac{2}{\beta}\langle f - u_1, \Delta\hat{p}\rangle\right\} = \left\{\|\nabla\Delta\tilde{p}\|^2 - \frac{2}{\beta}\langle f - u_1, \Delta\tilde{p}\rangle\right\}$ implying that $\tilde{\eta}_{i,j} = \frac{\hat{p}_{i,j}-\tilde{p}_{i,j}}{\tau} = 0$ for every i, j. Therefore, $\tilde{p} = \hat{p}$ and

$$-\Delta\left(\Delta^2\tilde{p} + \frac{(f-u_1)}{\beta}\right) + \left|\Delta\left(\Delta^2\tilde{p} + \frac{(f-u_1)}{\beta}\right)\right|\tilde{p} = 0 \tag{57}$$

the optimality equation for a solution minimizing problem (47). Therefore, $\Delta\tilde{p}$ is the solution to problem (47). Since this solution is unique, the complete sequence $\{\Delta p^n\}$ converges to the solution of (47), Thus, the theorem is proved if we can show that $\kappa^2 \leq 512$.

By definition, $\kappa = \sup_{\|p\|\leq 1}\|\nabla\Delta P\|$. Thus, using the standard zero boundary conditions for $p_{i,j}$, we have:

$$
\begin{aligned}
\|\nabla\Delta p\|^2 &\leq \sum_{i,j} \left(\Delta p_{i,j}\right)_x^2 + \left(\Delta p_{i,j}\right)_y^2 \\
&= \sum_{i,j} \left(\Delta p_{i,j} - \Delta p_{i-1,j}\right)^2 + \left(\Delta p_{i,j} - \Delta p_{i,j-1}\right)^2 \\
&= \sum_{i,j} \left(p_{i+1,j} - 5p_{i,j} + 5p_{i-1,j} + p_{i,j+1} + p_{i,j-1} - p_{i-2,j} - p_{i-1,j+1} - p_{i-1,j-1}\right)^2 \\
&\quad + \left(p_{i+1,j} - 5p_{i,j} + 5p_{i-1,j} + p_{i,j+1} + p_{i,j-1} - p_{i-2,j} - p_{i-1,j+1} - p_{i-1,j-1}\right)^2 \\
&\leq 16\sum_{i,j} \left(p_{i+1,j}^2 + 5p_{i,j}^2 + 5p_{i-1,j}^2 + p_{i,j+1}^2 + p_{i,j-1}^2 + p_{i-2,j}^2 + p_{i-1,j+1}^2 + p_{i-1,j-1}^2\right) \\
&\qquad + \left(p_{i+1,j}^2 + 5p_{i,j}^2 + 5p_{i-1,j}^2 + p_{i,j+1}^2 + p_{i,j-1}^2 + p_{i-2,j}^2 + p_{i-1,j+1}^2 + p_{i-1,j-1}^2\right) \\
&\leq 512\|p\|^2.
\end{aligned}
$$

Thus, $\kappa^2 \leq 512$. $\Diamond$

Remark The condition that $\tau \leq 1/512$ may seem restrictive, however, if we consider the existing time marching methods for solving the CEP–H^{-1} model, this may not be the case. Such time marching methods can give rise to a 6-th order non-linear equation (with CFL restrictions). More precisely, the Euler-Lagrange equation from the regularized minimization problem (40) amounts to solving

$$-\alpha\Delta\left(\frac{\Delta u_2}{\sqrt{(\Delta u_2)^2+\beta^2}}\right) - \frac{1}{\lambda}\Delta^{-1}\left(f-u_1-u_2\right) = 0; \qquad \frac{\partial \Delta u_2}{\partial n}|_{\partial\Omega} = 0, \quad \frac{\partial \Delta^2 u_2}{\partial n}|_{\partial\Omega} = 0. \tag{58}$$

Instead of directly solving (58), one can use the same technique as in [18] and apply the Laplacian to both sides of the equation to obtain

$$-\alpha\Delta^2\left(\frac{\Delta u_2}{\sqrt{(\Delta u_2)^2+\beta^2}}\right) - \frac{1}{\lambda}\left(f-u_1-u_2\right) = 0; \qquad \frac{\partial \Delta u_2}{\partial n}|_{\partial\Omega} = 0, \quad \frac{\partial \Delta^2 u_2}{\partial n}|_{\partial\Omega} = 0, \tag{59}$$

which can be solved by driving to steady state

$$\frac{\partial u}{\partial t} = \alpha\Delta^2\left(\frac{\Delta u_2}{\sqrt{(\Delta u_2)^2+\beta^2}}\right) + \frac{1}{\lambda}\left(f-u_1-u_2\right) = 0; \qquad \frac{\partial \Delta u_2}{\partial n}|_{\partial\Omega} = 0, \quad \frac{\partial \Delta^2 u_2}{\partial n}|_{\partial\Omega} = 0. \tag{60}$$

Equation (60) is a non-linear sixth order equation whose practicality can be limited by the small time steps needed to solve this equation. Moreover, the stiffness of solving this equation is compounded when the regularization parameter β is chosen small. Moreover, a proof of convergence for solving such an equation by artificial time marching has not been provided. In contrast, the previous condition on τ for the dual method may not seem so restrictive.

Of course, a dual method can also be formulated to solve for the discontinuous component u_1 in the minimization problem (41). Such a method was introduced by the authors in [2], and we pursue this approach with slight modification. Let us consider the following primal-dual formulation for (41):

$$\inf_{u_1}\sup_{\boldsymbol{\xi}}\left\{\int_\Omega u_1 \mathrm{div}(\boldsymbol{\xi})d\mathbf{x} + \frac{1}{2\lambda}\int_\Omega |\nabla\Delta^{-1}\left(f-u_1-u_2\right)|^2 d\mathbf{x} \;\mid\; \boldsymbol{\xi}\in C_c^1(\Omega;\mathbb{R}^2),\ |\boldsymbol{\xi}(\mathbf{x})| \leq 1\ \forall\ \mathbf{x}\in\Omega\right\} \tag{61}$$

where $\boldsymbol{\xi}$ is a vector valued function, $\boldsymbol{\xi} : \Omega \to \Omega \times \Omega$. The above equation (61), is convex in u_1 and concave (linear) in $\boldsymbol{\xi}$, thus, swapping the inf and sup and setting $v = \mathrm{div}(\boldsymbol{\xi})$ yields:

$$\sup_{v, v=\mathrm{div}(\boldsymbol{\xi})} \inf_{u_1} \left\{ \int_\Omega u_1 v d\mathbf{x} + \frac{1}{2\lambda} \int_\Omega |\nabla \Delta^{-1} (f - u_1 - u_2)|^2 d\mathbf{x} \;\middle|\; \boldsymbol{\xi} \in C_c^1(\Omega; \mathbb{R}^2),\ |\boldsymbol{\xi}(\mathbf{x})| \le 1 \ \forall\ \mathbf{x} \in \Omega \right\}. \tag{62}$$

Then, for each fixed v, the quantity

$$\inf_{u_1} \left\{ G(u_1) = \int_\Omega u_1 v d\mathbf{x} + \frac{1}{2\lambda} \int_\Omega |\nabla \Delta^{-1} (f - u_1 - u_2)|^2 d\mathbf{x} \right\} \tag{63}$$

yields a minimizer u_1: $u_1 = f - u_2 + \lambda \Delta v$. Substituting this expression for u_1 back into (62) and once again using the fact that $\sup \{G(\cdot)\} = -\inf \{-G(\cdot)\}$ yields the following full dual minimization problem with respect to v:

$$-\inf_{v, v=\mathrm{div}(\boldsymbol{\xi})} \left\{ \frac{\lambda}{2} \int_\Omega |\nabla v|^2 d\mathbf{x} - \int_\Omega (f - u_2) v d\mathbf{x} \;\middle|\; \boldsymbol{\xi} \in C_c^1(\Omega; \mathbb{R}^2),\ |\boldsymbol{\xi}(\mathbf{x})| \le 1 \ \forall\ \mathbf{x} \in \Omega \right\}. \tag{64}$$

Since we are only concerned with $v = \mathrm{div}(\boldsymbol{\xi})$, problem (64) can be reformulated as:

$$\inf_{\boldsymbol{\xi}} \left\{ \frac{\lambda}{2} \int_\Omega |\nabla \mathrm{div}(\boldsymbol{\xi})|^2 d\mathbf{x} - \int_\Omega (f - u_2) \mathrm{div}(\boldsymbol{\xi}) d\mathbf{x} \;\middle|\; \boldsymbol{\xi} \in C_c^1(\Omega; \mathbb{R}^2),\ |\boldsymbol{\xi}(\mathbf{x})| \le 1 \ \forall\ \mathbf{x} \in \Omega \right\}. \tag{65}$$

In the discrete setting, equation (65) can be set as a constrained minimization problem with inequality constraints:

$$\min_{\boldsymbol{p}, |\boldsymbol{p}| \le 1} \left\{ \frac{\lambda}{2} \int_\Omega |\nabla \mathrm{div}(\boldsymbol{p})|^2 d\mathbf{x} - \int_\Omega (f - u_2) \mathrm{div} \boldsymbol{p} d\mathbf{x} \right\} \tag{66}$$

whose optimality conditions read:

$$\nabla (f - u_2)_{i,j} + \lambda \nabla \Delta \mathrm{div}(\boldsymbol{p})_{i,j} + \alpha_{i,j} \boldsymbol{p}_{i,j} = \mathbf{0} \tag{67}$$

where $\alpha_{i,j}$ are the Lagrange Multipliers, and by complementary slackness, either $\alpha_{i,j} = 0$ (where $\nabla (f - u_2)_{i,j} + \lambda \nabla \Delta \mathrm{div}(\boldsymbol{p})_{i,j}$ is also 0) and $|\boldsymbol{p}_{i,j}| < 1$ or $\alpha_{i,j} > 0$ and $|\boldsymbol{p}_{i,j}| = 1$. Here, we once again need mention that the approach of solving a similar equation arising from the ROF model in the dual framework was pursued in [6, 12]. Again, using the observation and essential contribution in [7], we see that in either case, the Lagrange multipliers are:

$$\alpha_{i,j} = |\nabla (f - u_2)_{i,j} + \lambda \nabla \Delta \mathrm{div}(\boldsymbol{p})_{i,j}|$$

and the Lagrange multiplier (optimality) equation (67) reduces to:

$$\boldsymbol{A}(\boldsymbol{p})_{i,j} + |\boldsymbol{A}(\boldsymbol{p})_{i,j}| \boldsymbol{p}_{i,j} = \mathbf{0}$$

where $\boldsymbol{A}(\boldsymbol{p})_{i,j} = \nabla (\frac{f - u_2}{\lambda})_{i,j} + \nabla \Delta \mathrm{div}(\boldsymbol{p})_{i,j}$. This equation can be solved by the semi-implicit gradient descent (fixed point) iteration scheme introduced in [2, 7]:

$$\boldsymbol{p}^{n+1} = \boldsymbol{p}^n - \tau \left(\boldsymbol{A}_{i,j}^n + |\boldsymbol{A}_{i,j}^n| \boldsymbol{p}_{i,j}^{n+1} \right)$$

where $\boldsymbol{A}_{i,j}^n = \nabla (\frac{f - u_2}{\lambda})_{i,j} + \nabla \Delta \mathrm{div}(\boldsymbol{p}^n)_{i,j}$. Thus, the final iteration method reduces to the explicit scheme:

$$\boldsymbol{p}^0 = \mathbf{0}, \quad \boldsymbol{p}_{i,j}^{n+1} = \frac{\boldsymbol{p}_{i,j}^n - \tau \left(\nabla \left(\Delta \mathrm{div}(\boldsymbol{p}^n) + \frac{f - u_2}{\lambda} \right) \right)_{i,j}}{1 + \tau \left| \left(\nabla \left(\Delta \mathrm{div}(\boldsymbol{p}^n) + \frac{f - u_2}{\lambda} \right) \right)_{i,j} \right|}$$

where $f - u_2 + \lambda \Delta \boldsymbol{p}^n \longrightarrow \tilde{u_1}$ as $n \longrightarrow \infty$ for τ small enough, with $\tilde{u_1}$ a solution to (41).

Theorem 3.2 Let $\tau < 1/64$. Then, $v^n = \mathrm{div}(\boldsymbol{p}^n)$ converges to the solution of the minimization problem (66) as $n \longrightarrow \infty$.

Proof. The proof follows in the same manner as in Theorems 2.1 and 3.1. Fix $n \geq 0$ and set $\boldsymbol{\eta} = \frac{\boldsymbol{p}^{n+1} - \boldsymbol{p}^n}{\tau}$. Then,

$$\begin{aligned} \|\nabla \mathrm{div}(\boldsymbol{p}^{n+1})\|^2 - \frac{2}{\lambda} \left\langle (f - u_2), \mathrm{div}(\boldsymbol{p}^{n+1}) \right\rangle \quad &\leq \quad \|\nabla \mathrm{div}(\boldsymbol{p}^n)\|^2 - \frac{2}{\lambda} \left\langle (f - u_2), \mathrm{div}(\boldsymbol{p}^n) \right\rangle \\ &+ \quad \tau \left(2 \left\langle \nabla \left(\Delta \mathrm{div}(\boldsymbol{p}^n) + \frac{(f - u_2)}{\lambda} \right), \boldsymbol{\eta} \right\rangle + \tau \kappa^2 \|\boldsymbol{\eta}\|^2 \right) \end{aligned} \tag{68}$$

where $\|\boldsymbol{\eta}\|^2 = \langle \boldsymbol{\eta}, \boldsymbol{\eta} \rangle$ and κ denotes the norm of the operator $\nabla \mathrm{div} : \Omega \to \Omega \times \Omega$ to be computed shortly. Let $\boldsymbol{A}^n_{i,j} = \nabla \left(\Delta \mathrm{div}(\boldsymbol{p}^n) + \frac{(f - u_2)}{\lambda} \right)$. Now,

$$2 \left\langle \boldsymbol{A}^n, \boldsymbol{\eta} \right\rangle + \kappa^2 \tau \|\boldsymbol{\eta}\|^2 = \sum_{i,j=1}^{N} 2 \boldsymbol{\eta}_{i,j} \cdot \boldsymbol{A}^n_{i,j} + \tau \kappa^2 |\boldsymbol{\eta}_{i,j}|^2 \tag{69}$$

and the quantity $\boldsymbol{\eta}_{i,j} = -\boldsymbol{A}^n_{i,j} - \boldsymbol{\varrho}_{i,j}$ with $\boldsymbol{\varrho}_{i,j} = |\boldsymbol{A}^n_{i,j}| \boldsymbol{p}^{n+1}_{i,j}$. Therefore, for each i, j

$$2 \boldsymbol{\eta}_{i,j} \cdot \boldsymbol{A}^n_{i,j} + \kappa^2 \tau |\boldsymbol{\eta}_{i,j}|^2 = \left(\tau \kappa^2 - 1 \right) |\boldsymbol{\eta}_{i,j}|^2 + |\boldsymbol{\varrho}_{i,j}|^2 - |\boldsymbol{A}^n_{i,j}|^2. \tag{70}$$

Now, $|\boldsymbol{p}^{n+1}_{i,j}| \leq 1$ implies that $|\boldsymbol{\varrho}_{i,j}| \leq |\boldsymbol{A}^n_{i,j}|$. Thus, $|\boldsymbol{\varrho}_{i,j}|^2 \leq |\boldsymbol{A}^n_{i,j}|^2$. Hence, if $\left(\tau \kappa^2 - 1 \right) \leq 0$, i.e. $\tau \leq 1/\kappa^2$, the quantity

$$\|\nabla \mathrm{div}(\boldsymbol{p}^n)\|^2 - \frac{2}{\lambda} \left\langle (f - u_2), \mathrm{div}(\boldsymbol{p}^n) \right\rangle$$

is decreasing as n increases as long as $\boldsymbol{\eta} \neq \mathbf{0}$. If $\boldsymbol{\eta} = \mathbf{0}$, then $\boldsymbol{p}^{n+1} = \boldsymbol{p}^n$. A detailed analysis also shows that the energy still decreases in the case when $\kappa^2 \tau = 1$.

Now, set $L = \lim_{n \to \infty} \left\{ \|\nabla \mathrm{div}(\boldsymbol{p}^n)\|^2 - \frac{2}{\lambda} \left\langle (f - u_2), \mathrm{div}(\boldsymbol{p}^n) \right\rangle \right\}$ and let $\{\boldsymbol{p}^{n_q}\}$ be a convergent subsequence with limit $\tilde{\boldsymbol{p}}$ and let $\hat{\boldsymbol{p}} = \lim_{n \to \infty} \boldsymbol{p}^{n_q + 1}$. Then, we have

$$\hat{\boldsymbol{p}}_{i,j} = \frac{\tilde{\boldsymbol{p}}_{i,j} + \tau \nabla \left(\Delta \mathrm{div}(\tilde{\boldsymbol{p}}) + \frac{(f - u_2)}{\lambda} \right)_{i,j}}{1 + \tau \left| \nabla \left(\Delta \mathrm{div}(\tilde{\boldsymbol{p}}) + \frac{(f - u_2)}{\lambda} \right)_{i,j} \right|}. \tag{71}$$

Repeating the previous calculations and taking limits yields

$$\|\nabla \mathrm{div}(\hat{\boldsymbol{p}})\|^2 - \frac{2}{\lambda} \left\langle (f - u_2), \mathrm{div}(\hat{\boldsymbol{p}}) \right\rangle \ \leq \ \|\nabla \mathrm{div}(\tilde{\boldsymbol{p}})\|^2 - \frac{2}{\lambda} \left\langle (f - u_2), \mathrm{div}(\tilde{\boldsymbol{p}}) \right\rangle \ + \ \tau (\tau \kappa^2 - 1) \kappa^2 \|\boldsymbol{\eta}\|^2. \tag{72}$$

Now, $L = \left\{ \|\nabla \mathrm{div}(\hat{\boldsymbol{p}})\|^2 - \frac{2}{\lambda} \left\langle (f - u_2), \mathrm{div}(\hat{\boldsymbol{p}}) \right\rangle \right\} = \left\{ \|\nabla \Delta \tilde{\boldsymbol{p}}\|^2 - \frac{2}{\lambda} \left\langle (f - u_1), \mathrm{div}(\tilde{\boldsymbol{p}}) \right\rangle \right\}$ implying that $\boldsymbol{\eta}_{i,j} = \frac{\hat{\boldsymbol{p}}_{i,j} - \tilde{\boldsymbol{p}}_{i,j}}{\tau} = 0$ for every i, j. Therefore, $\tilde{\boldsymbol{p}} = \hat{\boldsymbol{p}}$ and

$$\nabla \left(\Delta \mathrm{div}(\tilde{\boldsymbol{p}}) + \frac{(f - u_2)}{\lambda} \right) + \left| \nabla \left(\Delta \mathrm{div}(\tilde{\boldsymbol{p}}) + \frac{(f - u_1)}{\lambda} \right) \right| \tilde{\boldsymbol{p}} = \mathbf{0} \tag{73}$$

the optimality equation for a minimizing solution of problem (66). Therefore, $\mathrm{div}(\tilde{\boldsymbol{p}})$ is the solution to problem (66). Since this solution is unique, the entire sequence $\{\mathrm{div}(\boldsymbol{p}^n)\}$ converges to the solution of (66). Thus, the theorem is proved if we can show that $\kappa^2 \leq 64$.

By definition, $\kappa = \sup_{\|\boldsymbol{p}\|\leq 1} \|\nabla \mathrm{div}(\boldsymbol{p})\|$. Thus, using the standard zero boundary conditions on $\boldsymbol{p}_{i,j}$, we have

$$\begin{aligned}
\|\nabla \mathrm{div}(\boldsymbol{p})\|^2 &\leq \sum_{i,j} \left(\mathrm{div}(\boldsymbol{p})_{i,j}\right)_x^2 + \left(\mathrm{div}(\boldsymbol{p})_{i,j}\right)_y^2 \\
&= \sum_{i,j} \left((p^1_{i,j})_x + (p^2_{i,j})_y\right)_x^2 + \left((p^1_{i,j})_x + (p^2_{i,j})_y\right)_y^2 \\
&= \sum_{i,j} \left(p^1_{i,j} - p^1_{i-1,j} + p^2_{i,j} - p^2_{i,j-1}\right)_x^2 + \left(p^1_{i,j} - p^1_{i-1,j} + p^2_{i,j} - p^2_{i,j-1}\right)_x^2 \\
&= \sum_{i,j} \left\{\left(p^1_{i,j} - p^1_{i-1,j} + p^2_{i,j} - p^2_{i,j-1}\right) - \left(p^1_{i-1,j} - p^1_{i-2,j} + p^2_{i-1,j} - p^2_{i-1,j-1}\right)\right\}^2 \\
&\quad + \left\{\left(p^1_{i,j} - p^1_{i-1,j} + p^2_{i,j} - p^2_{i,j-1}\right) - \left(p^1_{i,j-1} - p^1_{i-1,j-1} + p^2_{i,j-1} - p^2_{i,j-2}\right)\right\}^2 \\
&\leq \sum_{i,j} 8\left\{(p^1_{i,j})^2 + (p^1_{i-1,j})^2 + (p^2_{i,j})^2 + (p^2_{i,j-1})^2 + (p^1_{i-1,j})^2 + (p^1_{i-2,j})^2 + (p^2_{i-1,j})^2 + (p^2_{i-1,j-1})^2\right\} \\
&\quad + 8\left\{(p^1_{i,j})^2 + (p^1_{i-1,j})^2 + (p^2_{i,j})^2 + (p^2_{i,j-1})^2 + (p^1_{i,j-1})^2 + (p^1_{i-1,j-1})^2 + (p^2_{i,j-1})^2 + (p^2_{i,j-2})^2\right\} \\
&\leq 64\|\boldsymbol{p}\|^2
\end{aligned}$$

Thus, $\kappa^2 \leq 64$. $\Diamond$

4 The CEP2–G, CEP2–E, and CEP2–UVW Models and Corresponding Fourth Order Dual Methods

In this section, we propose staircase reducing image decomposition models explicitly involving the Meyer norms along with novel fourth order dual methods for obtaining solutions.

4.1 The CEP2–G Model, Approximation, and a 4-th order Dual Method

The proposed model, *CEP2–G*, involving Meyer's G norm is a $u + v$, structure + texture, staircase reducing decomposition model. The additional property of staircase reduction occurs in the structural component u of the decomposition by incorporating the energy $\|\Delta u_2\|_1$ into the original CEP–G model (9). Thus, the CEP2–G model has the following formulation as energy minimization

$$\inf_{f=u+v,\ u=u_1+u_2} \left\{ \int_\Omega |\nabla u_1| + \alpha \int_\Omega |\Delta u_2| + \beta \|v\|_G \right\}. \tag{74}$$

In practice, the minimization of (74) is difficult due to the nature of the G norm. Nonetheless, we follow the authors approach in [1, 11] to introduce the following approximation to the energy (74) called the *CEP2–G* approximation:

$$\inf_{\{(u,v)\in\Omega\times\Omega,\ u=u_1+u_2\}} \left\{ \int_\Omega |\nabla u_1| + \alpha \int_\Omega |\Delta u_2| + J^*\left(\frac{v}{\mu}\right) + \frac{1}{2\lambda}\int_\Omega (f - u_1 - u_2 - v)^2\, d\mathbf{x} \right\}. \tag{75}$$

Using similar arguments as in [11], it follows that as $\lambda \longrightarrow 0$, minimizing the energy in (75) yields a solution to the CEP2–G model (74).

We give some preliminary definitions where, following the notation in [2, 11], the discrete G space can be defined as:

$$G = \{ v \in \Omega \ \mid \ \exists \ \boldsymbol{g} \in \Omega \times \Omega \text{ such that } v = \operatorname{div}(\boldsymbol{g}) \ \} \tag{76}$$

having norm

$$\|v\|_G = \inf \left\{ \|\boldsymbol{g}\|_\infty \ \mid \ v = \operatorname{div}(\boldsymbol{g}), \ \boldsymbol{g} = (g^1, g^2) \in Y, \ |\boldsymbol{g}_{i,j}| = \sqrt{(g^1_{i,j})^2 + (g^2_{i,j})^2} \ \right\}. \tag{77}$$

Let the set μB_G be denoted by:

$$\mu B_G = \{ v \in G \ \mid \ \|v\|_G \leq \mu \}. \tag{78}$$

One way of minimizing the energy (75) amounts to solving the following three minimization problems:

for u_1 and v fixed, find solution u_2 of:

$$\inf_{u_2} \left\{ \alpha \int_\Omega |\Delta u_2| + \frac{1}{2\lambda} \int_\Omega (f - u_1 - u_2 - v)^2 \, d\mathbf{x} \right\}, \tag{79}$$

for u_1 and u_2 fixed, find solution v of:

$$\inf_{v \in \mu B_G} \left\{ \int_\Omega (f - u_1 - u_2 - v)^2 \, d\mathbf{x} \right\}, \tag{80}$$

for u_2 and v fixed, find solution u_1 of:

$$\inf_{u_1} \left\{ \int_\Omega |\nabla u_1| + \frac{1}{2\lambda} \int_\Omega (f - u_1 - u_2 - v)^2 \, d\mathbf{x} \right\}. \tag{81}$$

A solution $\tilde{u_2}$ of (79) can be obtained by solving a dual formulation of this energy in much the same way as in the 4-th order energy (20) obtained from the CEP–L^2 model (4). Indeed, the primal-dual formulation of (79) follows as:

$$\inf_{u_2} \sup_{\xi} \left\{ \alpha \int_\Omega u_2 \Delta \xi d\mathbf{x} + \frac{1}{2\lambda} \int_\Omega (f - u_1 - u_2 - v)^2 d\mathbf{x} \mid \xi \in C^2_c(\Omega; \mathbb{R}), \ -1 \leq \xi \leq 1 \right\}. \tag{82}$$

where ξ is a scalar valued function, $\xi : \Omega \to \Omega$. The above problem (82) is equivalent to solving the following full dual problem:

$$\inf_{\xi} \left\{ \int_\Omega \left(\frac{\alpha\lambda}{2} (\Delta\xi)^2 - (f - u_1 - v)\Delta\xi \right) d\mathbf{x} \mid \xi \in C^2_c(\Omega; \mathbb{R}), \ -1 \leq \xi \leq 1 \right\}. \tag{83}$$

In the discrete setting, minimizing the above equation (83) amounts to solving the following constrained optimization problem with inequality constraints:

$$\min_{p, |p| \leq 1} \left\{ \int_\Omega \left(\frac{\alpha\lambda}{2} (\Delta p)^2 - (f - u_1 - v)\Delta p \right) d\mathbf{x} \right\} \tag{84}$$

whose solution can be obtained from the semi-implicit gradient descent (fixed point iteration):

$$p^0 = 0; \quad p^{n+1}_{i,j} = p^n_{i,j} - \tau \left(A^n_{i,j} + |A^n_{i,j}| p^{n+1}_{i,j} \right). \tag{85}$$

The scheme (85) then, reduces to the explicit iteration scheme:

$$p^0 = 0; \quad p^{n+1}_{i,j} = \frac{p^n_{i,j} - \tau A^n_{i,j}}{1 + \tau |A^n_{i,j}|}, \tag{86}$$

where $A^n_{i,j} = \Delta^2 p^n_{i,j} - \Delta \left(\frac{f - u_1 - v}{\alpha\lambda} \right)_{i,j}$ and $u^n_2 = f - u_1 - v - \alpha\lambda\Delta p^n \longrightarrow \tilde{u_2}$ as $n \longrightarrow \infty$, with $\tilde{u_2}$ a solution of (82).

Theorem 4.1 Let $\tau < 1/64$. Then, $v^n = \Delta p^n$ converges to the solution of the minimization problem (84) as $n \longrightarrow \infty$.

Proof. The proof follows in exactly the same manner as in the proof of Theorem 2.1 except with the quantity $\left\{ \int_\Omega \left(\frac{\alpha\lambda}{2} (\Delta p)^2 - (f - u_1 - v)\Delta p \right) d\mathbf{x} \right\}$ replacing the energy $\left\{ \int_\Omega \left(\frac{\alpha\lambda}{2} (\Delta p)^2 - (f - u_1)\Delta p \right) d\mathbf{x} \right\}$. $\Diamond$

Solving for the texture part v requires the minimization of problem (80) as introduced in [1], which is equivalent to the following minimization problem:

for u_1 and u_2 fixed, find a solution v of:

$$\inf_{\|\frac{v}{\mu}\|_G \le 1} \left\{ \frac{1}{2} \int_\Omega (f - u - v)^2 \, d\mathbf{x} \right\}. \tag{87}$$

One can get a handle on the G norm in the discrete setting since the constraint: $\|\frac{v}{\mu}\|_G \le 1$ in the above minimization amounts to finding $\boldsymbol{g}$ such that $v = \mu \mathrm{div}(\boldsymbol{g}),\ |\boldsymbol{g}| \le 1$. Thus, the problem in equation (87) amounts to solving the constrained minimization problem with inequality constraints:

$$\min_{|\boldsymbol{p}| \le 1} \left\{ \frac{1}{2} \int_\Omega (f - u - \mu \mathrm{div}(\boldsymbol{p}))^2 \, d\mathbf{x} \right\}. \tag{88}$$

The optimality conditions for this problem read:

$$-\nabla \left(\mu \mathrm{div}(\boldsymbol{p}) - (f - u_1 - u_2) \right)_{i,j} + \alpha_{i,j} \boldsymbol{p}_{i,j} = \mathbf{0}$$

where the $\alpha_{i,j}$'s denote the Lagrange multipliers connected to each constraint in (88). Again, as in section §2 and in [2, 7], the Lagrange multipliers $\alpha_{i,j}$ reduce to $\alpha_{i,j} = |\mu \mathrm{div}(\boldsymbol{p}) - (f - u_1 - u_2)|_{i,j}$, and the optimality equation then reduces to

$$-\boldsymbol{A}(\boldsymbol{p})_{i,j} + |\boldsymbol{A}(\boldsymbol{p})_{i,j}| \boldsymbol{p}_{i,j} = \mathbf{0}$$

where $\boldsymbol{A}(\boldsymbol{p})_{i,j} = \left(\mathrm{div}(\boldsymbol{p}) - \frac{f - u_1 - u_2}{\mu} \right)_{i,j}$. Once again, this equation can be solved by the semi-implicit gradient descent (fixed point) iteration introduced in [7, 1]:

$$\boldsymbol{p}^0 = \mathbf{0}, \quad \boldsymbol{p}^{n+1}_{i,j} = \frac{\boldsymbol{p}^n_{i,j} + \tau \boldsymbol{A}^n_{i,j}}{1 + |\boldsymbol{A}^n_{i,j}|}.$$

Here, $\boldsymbol{A}_{i,j}^n = \left(\mathrm{div}(\boldsymbol{p}^n) - \frac{f-u_1-u_2}{\mu}\right)_{i,j}$, and for $\tau \leq \frac{1}{8}$, $v^n = \mu\mathrm{div}(\boldsymbol{p}^n) \longrightarrow \tilde{v}$ as $n \longrightarrow \infty$, where $\tilde{v}$ is a solution to (87).

Solving for the discontinuous component u_1 requires the minimization of problem (81), and follows in much the same way as with the dual formulation of the ROF model [6, 12, 7]. Thus, (81) can be reformulated as the following problem:
for u_2 and v fixed, find solution u_1 of:

$$\inf_{u_1} \sup_{\boldsymbol{\xi}} \left\{ \int_\Omega u_1 \mathrm{div}(\boldsymbol{\xi}) + \frac{1}{2\lambda} \int_\Omega (f-u-v)^2 \, d\mathbf{x} \;\middle|\; \boldsymbol{\xi} \in C_c^1(\Omega;\mathbb{R}^2),\; |\boldsymbol{\xi}| \leq 1 \right\}. \tag{89}$$

The above primal-dual problem (89) is almost identical to problem (37) obtained from the CEP2–L^2 model for obtaining u_1. Now, problem (89), in the discrete setting, is equivalent to the following constrained full dual minimization problem with inequality constraints

$$\min_{\boldsymbol{p}, |\boldsymbol{p}| \leq 1} \left\{ \int_\Omega (\lambda \mathrm{div}(\boldsymbol{p}) - (f-u_2-v))^2 \right\} \tag{90}$$

which can be solved by the fixed point (gradient descent) iteration scheme introduced in [7]:

$$\boldsymbol{p}^0 = \mathbf{0}, \quad \boldsymbol{p}_{i,j}^{n+1} = \frac{\boldsymbol{p}_{i,j}^n + \tau \boldsymbol{A}_{i,j}^n}{1 + |\boldsymbol{A}_{i,j}^n|}.$$

Here, $\boldsymbol{A}_{i,j}^n = \nabla\left(\mathrm{div}(\boldsymbol{p}^n) - \frac{f-u_2-v}{\lambda}\right)_{i,j}$, so that for $\tau \leq \frac{1}{8}$, $u_1^n = f - u_2 - v - \lambda\mathrm{div}(\boldsymbol{p}^n) \longrightarrow \tilde{u_1}$ as $n \longrightarrow \infty$, where $\tilde{u_1}$ is a solution to (89).

4.2 The CEP2–E Model, Approximation, and a 4-th Order Dual Method

Of course, one can just as easily apply the dual methods used to solve the CEP2–G model (74) to the proposed *CEP2–E* model, $E = B_{-1,\infty}^\infty$:

$$\inf_{\{(u,v)\in\Omega\times\Omega,\; u=u_1+u_2\}} \left\{ \int_\Omega |\nabla u_1| + \alpha \int_\Omega |\Delta u_2| + \beta \|v\|_E \right\}. \tag{91}$$

Again, as with Meyer's original G norm model, the CEP–G model, and the CEP2–G model, problem (91) cannot be solved directly due to the nature of the E norm. However, we may consider the proposed *CEP2-E Approximation* to the above energy (91) based on the approximations in [2, 11]:

$$\inf_{\{(u,v)\in\Omega\times\Omega,\; u=u_1+u_2\}} \left\{ \int_\Omega |\nabla u_1| + \alpha \int_\Omega |\Delta u_2| + B^*\left(\frac{v}{\delta}\right) + \frac{1}{2\lambda} \int_\Omega (f-u-v)^2 \, d\mathbf{x} \right\}. \tag{92}$$

One way of minimizing the above energy (92) amounts to solving the following minimization problems:

for u_1 and v fixed, find solution u_2 of:

$$\inf_{u_2} \left\{ \alpha \int_\Omega |\Delta u_2| + \frac{1}{2\lambda} \int_\Omega (f-u-v)^2 \, d\mathbf{x} \right\}, \tag{93}$$

for u_2 and v fixed, find solution u_1 of:

$$\inf_{u_1}\left\{\int_\Omega |\nabla u_1| + \frac{1}{2\lambda}\int_\Omega (f-u-v)^2\, d\mathbf{x}\right\}, \tag{94}$$

for u_1 and u_2 fixed, find solution v of:

$$\inf_{v\in\delta B_E}\left\{\int_\Omega (f-u-v)^2\, d\mathbf{x}\right\}. \tag{95}$$

Minimizing (93) and (94) follow in exactly the same manner as the methods used above in the CEP2–G approximation (75). To find a minimizer $\tilde{v}$ of equation (95), we use the same method as in [2, 11]. Here, $\tilde{v}$ is given by $\tilde{v} = f - u_1 - u_2 - WST(f-u_1-u_2,\delta)$, where WST stands for the wavelet soft thresholding algorithm given in [8] with threshold δ.

4.3 The CEP2–UVW Model and a 4-th Order Dual Method

In this section, we propose a staircase reducing u+v+w, structure+texure+noise model respectively, based on the models in [2, 11], that incorporates a high order energy. Moreover, we propose a fourth order dual method for obtaining solutions to this model. The proposed model, called the *CEP2-UVW* model, has the following formulation:

$$\inf_{u_1,u_2,v,w}\left\{\int_\Omega \left\{|\nabla u_1| + \frac{\alpha}{2}|\Delta u_2|\right\} + J^*\left(\frac{v}{\mu}\right) + B^*\left(\frac{w}{\delta}\right) + \frac{1}{2\lambda}\int_\Omega (f-u_1-u_2-v-w)^2 d\mathbf{x}\right\}. \tag{96}$$

One way of minimizing the CEP2–UVW energy (96) amounts to solving the following minimization problems:

for u_1, v and w fixed, find solution u_2 of:

$$\inf_{u_2}\left\{\frac{\alpha}{2}\int_\Omega |\Delta u_2| + \frac{1}{2\lambda}\int_\Omega (f-u_1-u_2-v-w)^2\, d\mathbf{x}\right\}, \tag{97}$$

for u_2, v and w fixed, find solution u_1 of:

$$\inf_{u_1}\left\{\int_\Omega |\nabla u_1| + \frac{1}{2\lambda}\int_\Omega (f-u_1-u_2-v-w)^2\, d\mathbf{x}\right\}, \tag{98}$$

for u_1, u_2 and w fixed, find solution v of:

$$\inf_{v\in\mu B_G}\left\{\int_\Omega (f-u_1-u_2-v-w)^2\, d\mathbf{x}\right\}, \tag{99}$$

for u_1, u_2 and v fixed, find solution w of:

$$\inf_{w\in\delta B_E}\left\{\int_\Omega (f-u_1-u_2-v-w)^2\, d\mathbf{x}\right\}. \tag{100}$$

The piecewise smooth component u_2, found by minimizing (97), can also be found by solving the associated primal-dual formulation:

$$\inf_{u_2}\sup_{\xi}\left\{\alpha\int_\Omega u_2\Delta\xi d\mathbf{x} + \frac{1}{2\lambda}\int_\Omega (f-u_1-u_2-v-w)^2 d\mathbf{x} \mid \xi\in C_c^2(\Omega;\mathbb{R}),\ -1\le\xi\le 1\right\}. \tag{101}$$

In the discrete setting, minimizing the above equation (101) amounts to solving the following constrained full dual optimization problem with inequality constraints:

$$\min_{p,|p|\leq 1}\left\{\int_\Omega\left(\frac{\alpha\lambda}{2}(\Delta p)^2-(f-u_1-v-w)\Delta p\right)d\mathbf{x}\right\}. \tag{102}$$

A solution of (102) can be found in almost the exact same way as in the CEP2-G approximation (75) solver for $\tilde{u_2}$ which amounts to solving the iteration scheme:

$$p^0=0,\quad p^{n+1}_{i,j}=\frac{p^n_{i,j}-\tau A^n_{i,j}}{1+\tau|A^n_{i,j}|} \tag{103}$$

where $A^n_{i,j}=\Delta^2 p^n_{i,j}-\Delta\left(\frac{f-u_1-v-w}{\alpha\lambda}\right)_{i,j}$ and for $\tau\leq\frac{1}{64}$, $u_2^n=f-u_1-v-w-\alpha\lambda\Delta p^n\longrightarrow\tilde{u_2}$ as $n\longrightarrow\infty$, with $\tilde{u_2}$ a solution of (101).

The discontinuous component u_1 obtained by minimizing (98) can also be found in almost the exact manner as in the dual CEP2–G (75) solver for u_1. If we set $\boldsymbol{A}^n_{i,j}=\nabla\left(\mathrm{div}(\boldsymbol{p}^n)-\frac{f-u_2-v-w}{\lambda}\right)_{i,j}$, then the semi-implicit fixed point iteration scheme:

$$\boldsymbol{p}^0=\mathbf{0},\quad \boldsymbol{p}^{n+1}_{i,j}=\frac{\boldsymbol{p}^n_{i,j}+\tau\boldsymbol{A}^n_{i,j}}{1+|\boldsymbol{A}^n_{i,j}|}$$

has the property that, for $\tau\leq\frac{1}{8}$, $u_1^n=f-u_2-v-w-\lambda\mathrm{div}(\boldsymbol{p}^n)\longrightarrow\tilde{u_1}$ as $n\longrightarrow\infty$, where $\tilde{u_1}$ a solution of (98).

Lastly, the texture component v obtained from the minimization of (99) can also be found in almost the exact same way as in the dual CEP2–G (75) solver for v. If we set $\boldsymbol{A}^n_{i,j}=\left|\frac{f-u_1-u_2-w}{\mu}-\mathrm{div}(\boldsymbol{p}^n)\right|_{i,j}$, then the fixed point iteration:

$$\boldsymbol{p}^0=\mathbf{0};\quad \boldsymbol{p}^{n+1}_{i,j}=\frac{\boldsymbol{p}^n_{i,j}+\tau\boldsymbol{A}^n_{i,j}}{1+|\boldsymbol{A}^n_{i,j}|}$$

has the property that, for $\tau\leq\frac{1}{8}$, $v^n=\mu\mathrm{div}(\boldsymbol{p}^n)\longrightarrow\tilde{v}$ as $n\longrightarrow\infty$, $\tilde{v}$ a solution of (99).

Finally, the noise component w obtained by minimizing (100) can be found by computing $\tilde{w}=f-u_1-u_2-v-WST(f-u_1-u_2-v,\delta)$, where $WST(f-u_1-u_2-v)$ is wavelet soft thresholding of $f-u_1-u_2-v$ with threshold δ (see [2, 8]).

5 Numerical Experiments

5.1 1-D Results

Figure 2 illustrates the ability of the norm $\|\Delta\cdot\|_1$ to preserve discontinuities in the second derivative (e.g. kinks or ridges). We utilize the 1-d case to better demonstrate this phenomenon. Top left and right, clean and noisy signals are respectively observed, SNR=15. Middle left and right, recovered signals obtained from the CEP–L^2 and CEP2–L^2 models respectively. As expected behavior from the $\|\Delta\cdot\|_2^2$ norm, the observation can be made that the recovered signal from the CEP–L^2 model has no sharp corners. In contrast, the recovered signal obtained from the CEP2–L^2 model has better preserved corners which is expected from the utilization of the non-smooth energy. Comparable noise components are observed bottom left and right for the CEP–L^2 and CEP2–L^2 models respectively.

5.2 2-D Results

In this section, we demonstrate staircase reduction in both denoising and texture extraction applications. We will also compare the proposed models with some popular denoising and decomposition models.

In this first experiment, we illustrate staircase reduction for denoising applications. Exhibited, in Figure 3, clean and noisy images left and right respectively. For the observed image, $\sigma = 20$, σ^2 the variance of a Gaussian noise. Showcased in figure 4, top left and right, are the recovered image $u = u_1 + u_2$ and the removed noise $v = f - u_1 - u_2$ respectively obtained from the CEP2–L^2 model. Here, we observe no significant staicasing in u. In the same figure, bottom left and right, are the discontinuous and piecewise smooth components u_1 and u_2 respectively. Of course, a comparison should be made to the ROF model and in Figure 5, we observe, top left, the recovered image u obtained from the ROF model and bottom left, the recovered image $u = u_1 + u_2$, obtained from the CEP2–L^2 model. Staircasing can already be detected on Barbara's face and arms in the ROF component; particularly on the left side of her face (Barbara's face) and on her left forearm and right upper arm. In u obtained from the CEP2–L^2 Model, staircasing appears to be alleviated. Comparable noise components are observed in top and bottom right, the components $v = f - u$ and $f - u_1 - u_2$, obtained from the ROF and CEP2–L^2 models respectively. All the parameters have been chosen so that $\|v\|_2$ are the same for both models. In Figure 6, we showcase, left and right, zoom ins of the face in the recovered images u and $u = u_1 + u_2$, for the ROF and CEP2–L^2 models respectively. Here, prominent staircasing is observed on Barbara's face in the image obtained from the ROF model. Staircasing has been successfully reduced in the image obtained from the CEP2–L^2 model while sharp edges are maintained.

The next experiment compares the recovered image obtained from the dual method to that obtained from an artificial time marching method for the CEP2–L^2 model. In Figure 7, top and bottom left, we observe the recovered images $u = u_1 + u_2$ and u, obtained from the high order dual method and an artificial time marching method respectively. The images appear comparable with some very slight variation introduced from the β parameter used to regularize the non-smooth energies of the CEP2–L^2 model when utilizing time marching. Top right and bottom right, comparable noise components $v = f - u_1 - u_2$ and $v = f - u$, obtained from the dual and time marching methods are respectively observed.

The purpose of the next experiment is to ensure that the texture extraction properties of the CEP2–H^{-1} model are comparable to the OSV model while simultaneously reducing staircasing. In Figure 8 left, a clean Barbara image containing structural (geometric) and texture (oscillatory) components is observed. A noisy version of this image, $\sigma = 20$, σ^2 the variance of a Gaussian noise, is observed on the right. Figure 9, top left and right, exhibits the structural component $u = u_1 + u_2$ and the texture component $v = f - u_1 - u_2$ respectively obtained from the CEP2–H^{-1} model while the piecewise constant and smooth components u_1 and u_2 are observed bottom left and right respectively. Here, we make the observation that there is an absence of any significant staircasing in the structural component u. Moreover, the texture component appears to contain mostly oscillatory features. Of course, a comparison is in order, and in Figure 10, we compare the CEP2–H^{-1} and OSV Models. Here, we observe, top left and bottom left, the structural components u and $u = u_1 + u_2$, obtained from the OSV and CEP2–H^{-1} models respectively. Even without zooming in, staircasing can already be detected in the component obtained from the OSV model. This is particularly noticeable on the left side of Barbara's face (her left) and on her arms. Top right and bottom right are the corresponding texture components $v = f - u$ and $v = f - u_1 - u_2$, obtained from the OSV and CEP2–H^{-1} models respectively. These texture components appear to be comparable with mostly oscillatory features. To better illustrate staircasing, in Figure 11, we display some zoom ins of the structural components obtained from the OSV and CEP2–H^{-1} models. Left and right, zoom ins of the face from the structural component obtained from the OSV and CEP2–H^{-1} models respectively. In the OSV component, prominent staircasing can be observed on Barbara's face. In the CEP2–H^{-1} component, staircasing has been successfully reduced, while sharp edges are still maintained. Similar observations can be deduced from Figure 12, where the zoom ins of Barbara's upper arm and forearm are exhibited. Again, the parameters have been chosen so that $\|v\|_2$ are the same for both models.

In the final experiment, we compare the recovered image obtained from the high order dual method to that of an artificial time marching method for the CEP2–H^{-1} model. In Figure 13, top and bottom left, we observe the recovered images $u = u_1+u_2$ and u, obtained from the proposed dual method and an artificial time marching method respectively. The images appear comparable with some slight variation introduced from the β parameter used to regularize the non-smooth energies in the CEP2–H^{-1} model when utilizing time marching. We observe, top right and bottom right, comparable noise components $v = f - u_1 - u_2$ and $v = f - u$, obtained from the dual and time marching methods respectively.

6 Future Works

In this paper, we introduced new texture decomposition and restoration models incorporating fourth order non-smooth energies in image processing along with novel high order dual methods to obtain the corresponding solutions. Some future works include some even faster methods that exceed the current convergence rate of the fixed point methods utilized in this paper.

Acknowledgements

The authors would like to thank David Weisbart and Jean-Francois Aujol for their valuable comments and discussions.

References

[1] J.-F. Aujol, G. Aubert, L. Blanc-Feraud, A. Chambolle, Image decomposition: application to textured images and SAR images, Rapport de Recherche RR 4704, INRIA, January 2003.

[2] J.-F. Aujol and A. Chambolle, Dual Norms and Image Decomposition Models, Intl. J. Comp. Vis. 63:1 (2005), pp. 85–104.

[3] J.-F Aujol, G. Gilboa, T. F. Chan, and S. Osher, Structure-texture image decomposition - modeling, algorithms, and parameter selection, UCLA Cam Report 05-10 (2005).

[4] M. Bertalmio, L. Vese, G. Sapiro, and S. Osher, Simultaneous structure and texture image inpainting, IEEE Trans. Image Proc. 12:8 (2003), pp. 882–889.

[5] P. Blomgren, P. Mulet, T. Chan, and C. Wong, Total variation image restoration: numerical methods and extensions, Proceedings ICIP (1997), pp. 384–387.

[6] J. L. Carter, Dual methods for total variation–based image restoration, Ph.D. thesis (Advisor: T. F. Chan), UCLA (2001).

[7] A. Chambolle, An algorithm for total variation minimization and applications, JMIV 20 (2004), pp. 89–97.

[8] A. Chambolle, R. A. De Vore, N. Lee, B. J. Lucier, Nonlinear wavelet image processing: variational problems, compression, and noise removal through wavelet shrinkage. IEEE Trans. Image Proc. 7:3 (1998), pp. 319–335.

[9] A. Chambolle and P. Lions, Image recovery via total variation minimization and related problems, Numer. Math. 76:2 (1997), pp. 167–188.

[10] T. F. Chan and S. Esedoglu, Aspects of total variation regularized L^1 function approximation, UCLA CAM Report 04-07 (2004), (Accepted for publication in SIAM J. Appl. Math).

[11] T. F. Chan, S. Esedoglu, and F. E. Park, Image decomposition combining staircase reduction and texture extraction, UCLA CAM Report 05-18 (2005).

[12] T. F. Chan, G. Golub, and P. Mulet, A nonlinear primal-dual method for total variation based image restoration, SIAM J. Sci. Comp., 20 (1999), pp. 1964–1977.

[13] T. F. Chan, A. Marquina, and P. Mulet, High order total variation based image restoration, SIAM J. Sci. Comp., 22:2 (2000), pp. 503–516.

[14] T. F. Chan and F. Park, Data Dependent multiscale total variation based image decomposition and contrast preserving denoising, UCLA Cam Report 04-15 (2004).

[15] S. Esedoglu and S. Osher, Decomposition of images by the anisotropic Rudin-Osher-Fatemi model, Comm. Pure Appl. Math. 57 (2004), pp. 1609–1626.

[16] S. Levine, M. Ramsey, T. Misner, and S. Schwab, An adaptive model for image decomposition with applications to remote sensing, Duquesne Univ. Dept. of Math and Comp. Sci. Tech. Report 05-01 (2005).

[17] Y. Meyer, Oscillating patterns in image processing and nonlinear evolution equations (Lewis Memorial Lectures), AMS (2001).

[18] S. Osher, A. Sole, and L. Vese, Image decomposition and restoration using total variation minimization and the H^{-1} norm, Multiscale Model. Simul. 1:3 (2003), pp. 349–370.

[19] L. I. Rudin, S. Osher, and E. Fatemi, Nonlinear total variation based noise removal algorithms, Physica D 60 (1992), pp. 259–268.

[20] J. L. Starck, M. Elad, and D. L. Donoho, Image decomposition: separation of texture from piecewise smooth content, Proceedings SPIE 5207 (2003), pp. 571–582.

[21] E. Tadmor, S. Nezzar, and L. Vese, A multiscale image representation using hierarchical (BV, L^2) decompositions, Multiscale Model. Simul. 2:4 (2003), pp. 554–579.

[22] L. Vese and S. Osher, Modeling textures with total variation minimization and oscillating patterns in image processing, J. Math. Imaging Vision 20 (2004), pp. 7–18.

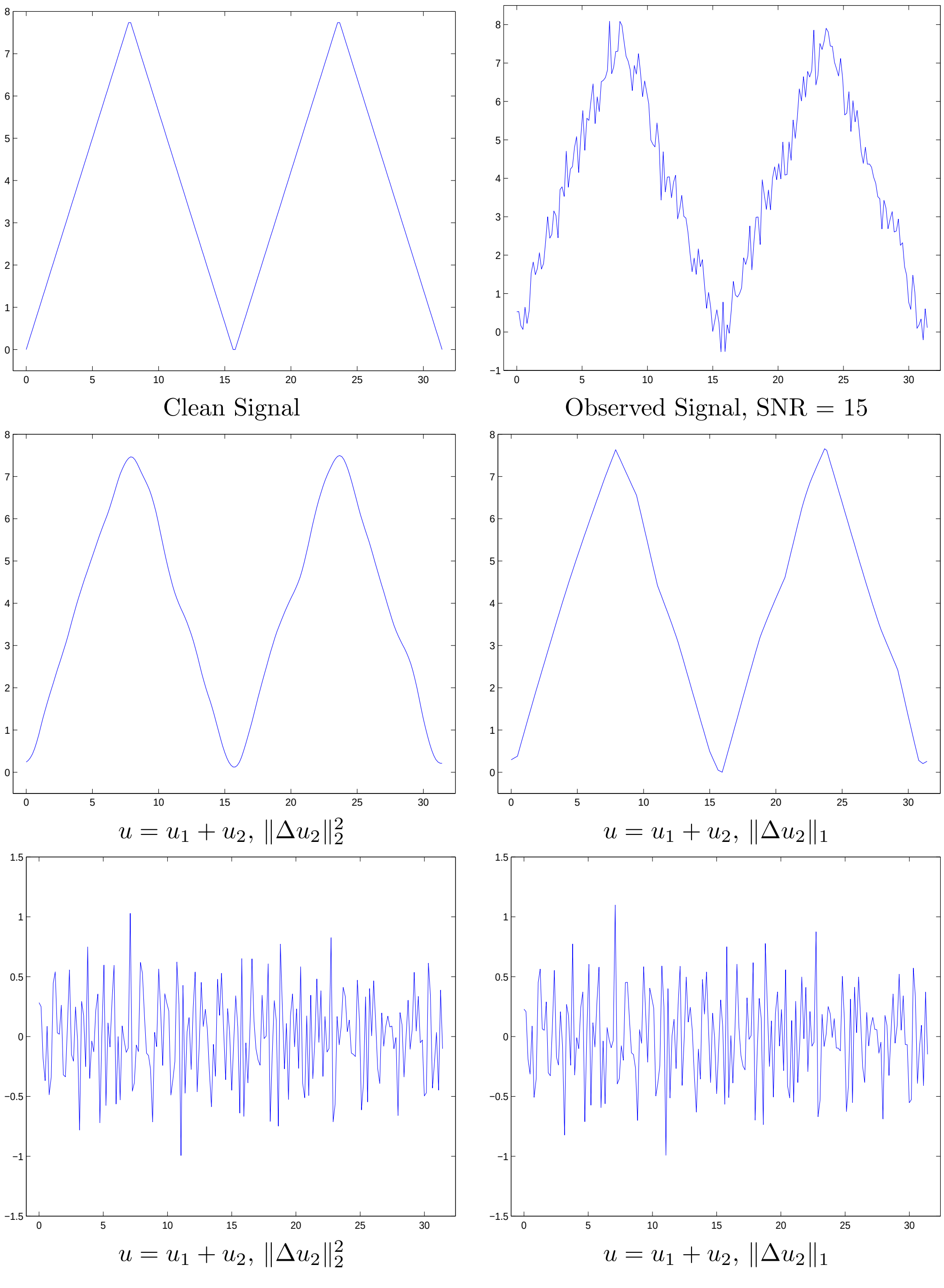

Figure 2: *Preservation of Discontinuities in the 2nd Derivative:* Top left and right, the clean and observed signals respectively. The SNR=15 for the observed signal. Middle left, recovered signal from the CEP–L^2 model. Here, we observe that the kinks (peaks) in the recovered image are rounded off. Middle right, recovered image from the proposed CEP2–L^2 model. In this case, the kinks are much better preserved. Bottom left and right, the noise components for the CEP–L^2 and CEP2–L^2 models respectively. The noise components appear comparable. Parameters have been chosen so that $\|v\|_2$ are the same for both models, $v = f - u_1 - u_2$.

Clean Image

Observed Image, $\sigma = 20$

Figure 3: *Clean and Nosy Image:* Left, clean image. Right, noisy observed image with Gaussian noise of variance σ^2, σ=20.

$u = u_1 + u_2$, CEP2–L^2 Model

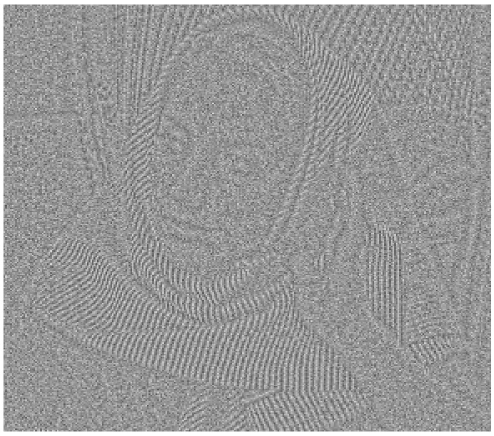

$v = f - u_1 - u_2$, CEP2–L^2 Model

u_1, CEP2–L^2 Model

u_2, CEP2–L^2 Model

Figure 4: *Image Denoising, CEP2–L^2 Model (17):* Top left, recovered image $u = u_1 + u_2$, obtained from the CEP2–L^2 Model utilizing the fourth order dual method. Top right, the removed noise $v = f - u_1 - u_2$. Bottom left and right, the piecewise constant u_1 and piecewise smooth u_2 regions respectively. No significant staircasing is observed in the recovered image $u = u_1 + u_2$.

u, ROF Model

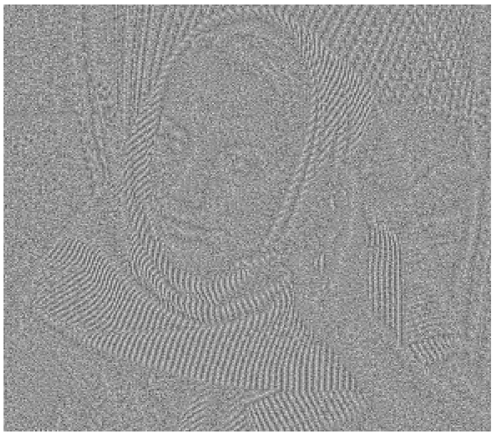

$v = f - u$, ROF Model

$u = u_1 + u_2$, CEP2–L^2 Model

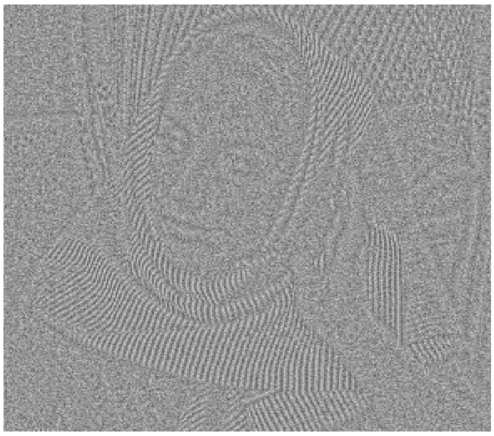

$v = f - u_1 - u_2$, CEP2–L^2 Model

Figure 5: *Comparison of the CEP2–L^2 Model (17) and the ROF Model:* Top left, recovered image u obtained from the ROF model. Staircasing can already be detected on Barbara's face and arms. Bottom left, recovered image $u = u_1 + u_2$, obtained from the CEP2–L^2 model. Staircasing appears to be alleviated. Top and bottom right, the noise components $v = f - u$ and $v = f - u_1 - u_2$, obtained from the ROF and CEP2–L^2 models respectively. Both noise components appear to be comparable and the parameters have been chosen so that $\|v\|_2$ are the same for both models.

Zoom of u, ROF Model   Zoom of $u = u_1 + u_2$, CEP2–L^2 Model

Figure 6: *Zoom In, Comparison of the CEP2–L^2 Model (17) and the ROF Model:* Left and right, zoom in of the face of the recovered images u and $u = u_1 + u_2$, obtained from the ROF and CEP2–L^2 models respectively. Prominent staircasing can be observed on Barbara's face in the image obtained from the ROF model. Staircasing has been successfully reduced in the image obtained from the CEP2–L^2 model while maintaining sharp edges.

$u = u_1 + u_2$, Dual

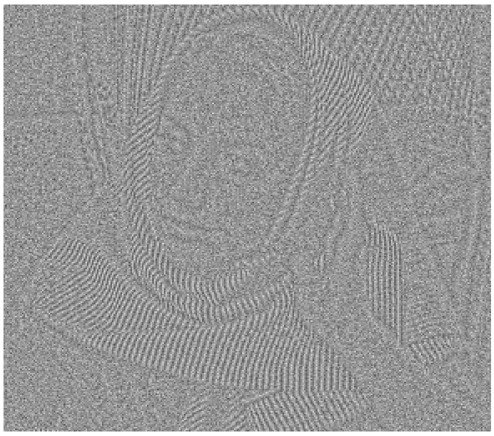

$v = f - u_1 - u_2$, Dual

$u = u_1 + u_2$, Time Marching

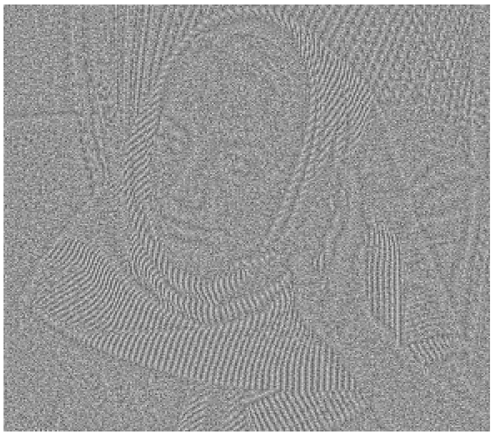

$v = f - u_1 - u_2$, Time Marching

Figure 7: *Dual Versus Artificial Time Marching, CEP2–L^2 Model (17):* Top left and bottom left, recovered images $u = u_1 + u_2$, obtained from the dual and artificial time marching methods respectively. Top right and bottom right, the noise components $v = f - u_1 - u_2$, obtained from the dual and artificial time marching methods respectively. Both structural u and noise v components are comparable.

Clean Image Observed Image, $\sigma = 20$

Figure 8: *Clean and Noisy Image:* Left, clean image containing both structural (geometric) and texture (oscillatory) features. Right, noisy observed image with Gaussian noise of variance σ^2, σ=20.

$u = u_1 + u_2$, CEP2–H^{-1} Model

$v = f - u_1 - u_2$, CEP2–H^{-1} Model

u_1

u_2

Figure 9: *Texture Decomposition, CEP2–H^{-1} Model (39):* Top left, the structural (geometric) component $u = u_1 + u_2$, obtained from the CEP2–H^{-1} Model utilizing the fourth order dual method. Top right, the texture component $v = f - u_1 - u_2$ where, mostly oscillatory features (texture) are visible. Bottom left and right, the piecewise constant u_1 and piecewise smooth u_2 regions respectively. Once again, as with the CEP2–L^2 model, no significant staircasing is observed in the structural component $u = u_1 + u_2$.

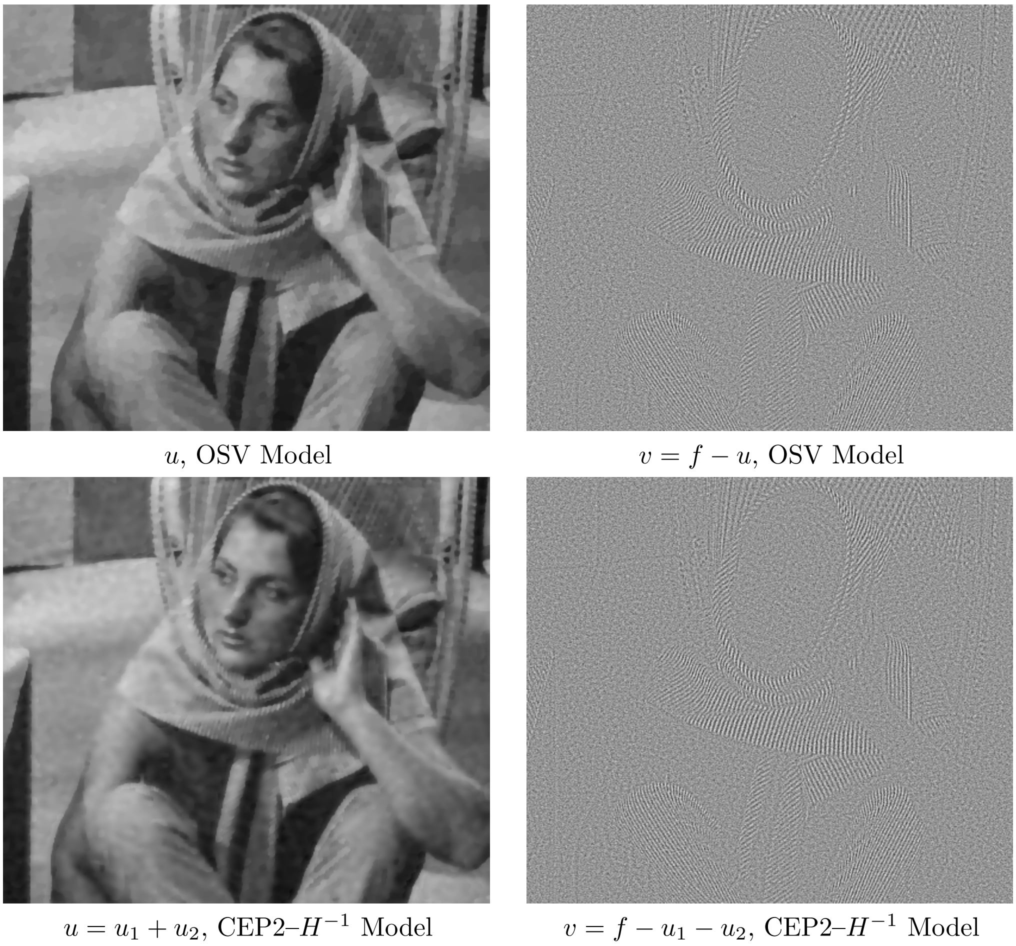

Figure 10: *Comparison of the CEP2–H^{-1} and OSV Models:* Top left and bottom left, structural components u and $u = u_1 + u_2$, obtained from the OSV and CEP2–H^{-1} models respectively. Top right and bottom right, the corresponding texture components $v = f - u$ and $v = f - u_1 - u_2$, obtained from the OSV and CEP2–H^{-1} models respectively . Without zooming in, staircasing can already be detected in the u component obtained from the OSV model. The texture components v are comparable for both models.

Zoom of u, OSV Model

Zoom of $u = u_1 + u_2$, CEP2-H^{-1} Model

Figure 11: *Comparison of the CEP2–H^{-1} and OSV Models, Zoom Ins:* Left and right, zoom in of face from the structural components u and $u = u_1 + u_2$, obtained from the OSV and CEP2–H^{-1} models respectively. Prominent staircasing is observed in the zoom of the component obtained from the OSV model. Staircasing is alleviated in the component obtained from the CEP2-H^{-1} model.

 

Zoom of u, OSV Model — Zoom of $u = u_1 + u_2$, CEP2–H^{-1} Model

 

Zoom of u, OSV Model — Zoom of $u = u_1 + u_2$, CEP2–H^{-1} Model

Figure 12: *Comparison of the CEP2–H^{-1} and OSV Models, Zoom Ins:* Top left and right, zoom in of the arm from the structural components u and $u = u_1 + u_2$, obtained from the OSV and CEP2–H^{-1} models respectively. Prominent staircasing is observed in the zoom of the component obtained from the OSV model, particularly near the upper arm. Staircasing has been successfully alleviated in the component obtained from the CEP2-H^{-1} model. Similar observations can be made from the zoom ins of the forearm seen bottom left and right, for the components u and $u = u_1 + u_2$, obtained from the OSV and CEP2–H^{-1} models respectively.

$u = u_1 + u_2$, Dual

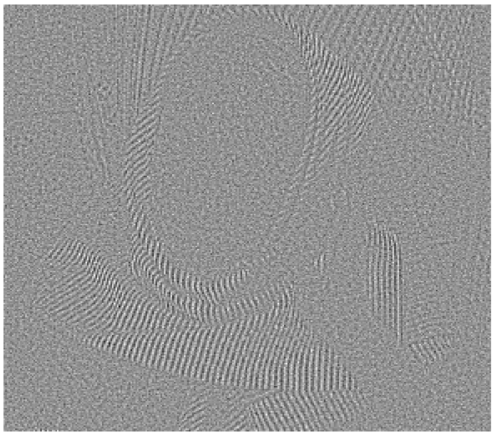

$v = f - u_1 - u_2$, Dual

$u = u_1 + u_2$, Time Marching

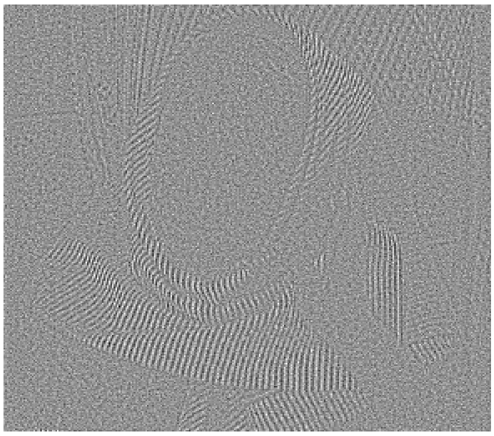

$v = f - u_1 - u_2$, Time Marching

Figure 13: *Dual Versus Time Marching, CEP2–H^{-1} Model (39):* Top left and bottom left, structural components $u = u_1 + u_2$, obtained from the dual and artificial time marching methods respectively. Top right and bottom right, the texture components $v = f - u_1 - u_2$, obtained from the dual and artificial time marching methods respectively. Both structural u and noise v components are comparable.